Article

Cell

Long-Distance Cooperative and Antagonistic RNA Polymerase Dynamics via DNA Supercoiling

Graphical Abstract

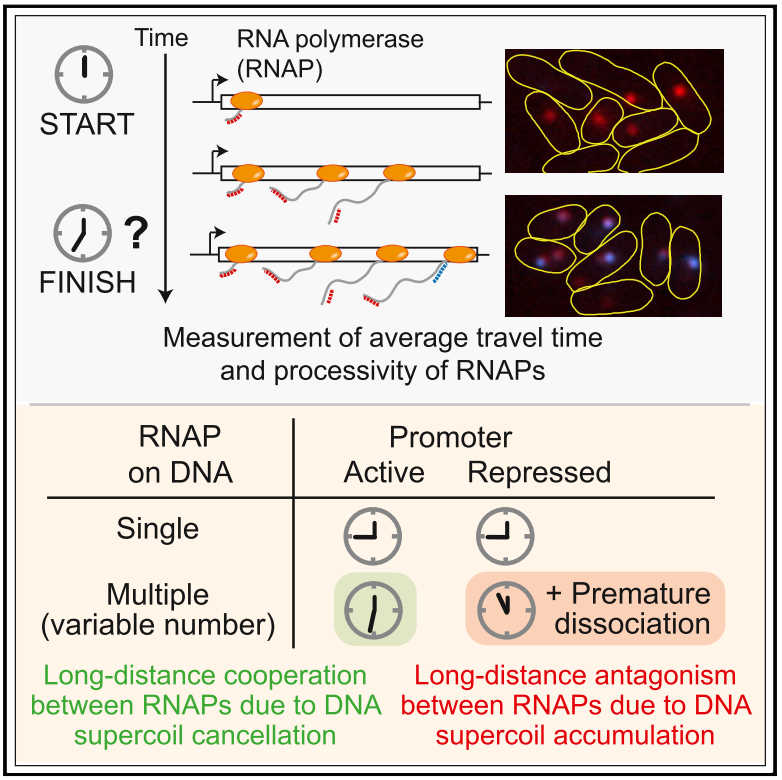

Highlights

- Multiple RNA polymerases (RNAPs) translocate faster than a single RNAP
- Cooperation between RNAPs is not additive and occurs over long distances
- Promoter repression leads to antagonistic dynamics and premature dissociation of RNAPs
- Transcription-coupled DNA supercoiling causes these long-distance RNAP dynamics

Authors

Sangjin Kim, Bruno Beltran, Irnov Irnov, Christine Jacobs-Wagner

Correspondence

sangjin@illinois.edu (S.K.), christine.jacobs-wagner@yale.edu (C.J.-W.)

In Brief

Supercoiling introduced into DNA strands during the process of transcription influences other transcribing RNA polymerases over long distances, providing a physical basis for cooperative and antagonistic polymerase group behaviors.

Kim et al., 2019, Cell *179*, 106–119
September 19, 2019
https://doi.org/10.1016/j.cell.2019.08.033

CellPress

Cell

Article

Long-Distance Cooperative and Antagonistic RNA Polymerase Dynamics via DNA Supercoiling

Sangjin Kim,[1,2,3,5,*] Bruno Beltran,[1,3,6] Irnov Irnov,[1,2,3] and Christine Jacobs-Wagner[1,2,3,4,7,8,*]
[1]Microbial Sciences Institute, Yale University, West Haven, CT 06516, USA
[2]Department of Molecular, Cellular and Developmental Biology, Yale University, New Haven, CT 06511, USA
[3]Howard Hughes Medical Institute, Yale University, New Haven, CT 06536, USA
[4]Department of Microbial Pathogenesis, Yale School of Medicine, New Haven, CT 06536, USA
[5]Present address: Department of Physics, Center for the Physics of Living Cells and Institute for Genomic Biology, University of Illinois at Urbana-Champaign, Urbana, IL 61801, USA
[6]Present address: Biophysics Program, Stanford University, Stanford, CA 94305, USA
[7]Present address: Department of Biology and Stanford ChEM-H, Stanford University, Stanford, CA 94305, USA
[8]Lead Contact
*Correspondence: sangjin@illinois.edu (S.K.), christine.jacobs-wagner@yale.edu (C.J.-W.)
https://doi.org/10.1016/j.cell.2019.08.033

SUMMARY

Genes are often transcribed by multiple RNA polymerases (RNAPs) at densities that can vary widely across genes and environmental conditions. Here, we provide *in vitro* and *in vivo* evidence for a built-in mechanism by which co-transcribing RNAPs display either collaborative or antagonistic dynamics over long distances (>2 kb) through transcription-induced DNA supercoiling. In *Escherichia coli*, when the promoter is active, co-transcribing RNAPs translocate faster than a single RNAP, but their average speed is not altered by large variations in promoter strength and thus RNAP density. Environmentally induced promoter repression reduces the elongation efficiency of already-loaded RNAPs, causing premature termination and quick synthesis arrest of no-longer-needed proteins. This negative effect appears independent of RNAP convoy formation and is abrogated by topoisomerase I activity. Antagonistic dynamics can also occur between RNAPs from divergently transcribed gene pairs. Our findings may be broadly applicable given that transcription on topologically constrained DNA is the norm across organisms.

INTRODUCTION

RNA polymerases (RNAPs) carry out the first step of gene expression by transcribing DNA into RNA. This process is essential for most aspects of cellular life and, as a result, has been extensively studied for decades. For instance, *in vitro* studies have yielded a wealth of knowledge on how a single RNAP translocates on a DNA template during elongation (Bai et al., 2006; Larson et al., 2011). Inside cells, genes are often transcribed simultaneously by multiple RNAPs. How transcription occurs and is regulated in the context of this multiplicity is less clear. This is complicated by the fact that, although transcription by multiple RNAPs is common, the number of RNAPs vary widely from gene to gene (Larson et al., 2014; Mayer et al., 2015; Min et al., 2011; Mokry et al., 2012; Mooney et al., 2009; Pelechano et al., 2009; Vijayan et al., 2011; Wade and Struhl, 2004), which in part reflects the broad range of promoter strengths across genes. Moreover, promoter activity and thus RNAP density can change dynamically in response to a changing environment or during development.

It is known that two RNAPs can cooperate and affect each other's speed when they come close or collide (Le and Wang, 2018). *In vitro* and *in vivo* experiments have shown that a trailing RNAP can assist a leading RNAP to overcome a sequence-specific pause or a roadblock on the DNA (e.g., a nucleosome) when they run into each other (Epshtein and Nudler, 2003; Epshtein et al., 2003; Jin et al., 2010; Kulaeva et al., 2010; Saeki and Svejstrup, 2009). This close-distance cooperation occurs because long pauses often result in RNAP backtracking, and a trailing RNAP can effectively "push" a backtracked RNAP forward. A study in *Escherichia coli* has suggested that RNAP "pushes" can be cumulative, based on the observation that a gene driven by a strong synthetic promoter (T7 A1) displays faster elongation when the promoter is maximally induced compared to partially repressed (Epshtein and Nudler, 2003). This result led to the conclusion that the rate of transcription elongation scales with the rate of transcription initiation. Because RNAP pushes rely on RNAP interactions, cooperation is thought to be most effective for genes with very strong promoters (Epshtein and Nudler, 2003; Proshkin et al., 2010; Saeki and Svejstrup, 2009), such as ribosomal genes, where elongating RNAPs form long convoys due to frequent back-to-back loading onto the DNA (Voulgaris et al., 1999). Consistent with this idea, ribosomal genes display faster elongation rates than most genes (Condon et al., 1993; Ryals et al., 1982; Voulgaris et al., 1999), although other mechanisms are likely to contribute to this difference (Vogel and Jensen, 1994, 1997).

Recently, another model was proposed on a theoretical basis to explain how higher initiation rates could lead to faster elongation (Heberling et al., 2016). In this mathematical model, RNAPs affect each other's speed, not via a physical push but via an RNAP-induced torque that acts on non-touching but still closely spaced RNAPs by effectively pushing them from the back and

"pulling" them from the front. The proposed torque depends on the distance between these RNAPs and the rate of transcription initiation. As a result, closely spaced RNAPs on highly expressed genes are the most affected. This "push-pull" model has also been theorized to explain how RNAPs loaded close to each other can translocate at the same velocity and travel as a convoy during elongation (Tantale et al., 2016).

Regardless of the model (push or push-pull), it remains unclear whether a scaling relationship between initiation and elongation rates applies across most physiological levels of gene expression. The strength of the fully induced T7 A1 promoter, which was used in the experiments that led to the scaling idea (Epshtein and Nudler, 2003), is similar to that of ribosomal promoters (Deuschle et al., 1986). Comparatively, the vast majority of genes across cell types have much weaker promoters (Bon et al., 2006; Pelechano et al., 2010; Schwanhäusser et al., 2011; Taniguchi et al., 2010), reducing the probability of interactions between RNAPs. Whether RNAPs can affect each other under these relevant contexts of lower RNAP density remains unknown.

In this study, we provide evidence that the rate of transcription elongation does not change with the rate of transcription initiation under a large range of physiological gene expression levels, which is inconsistent with existing models of RNAP cooperation. However, to our surprise, the efficiency of transcription elongation of already-transcribing RNAPs becomes compromised when the loading of new RNAPs stops due to environmentally induced promoter repression. This occurs independently of convoy formation or promoter strength, as long as the DNA template is transcribed by more than one RNAP. These contrasting results are reconciled by a mechanism in which RNAPs affect each other over remarkably long distances (>2 kb), either collaboratively or antagonistically, through transcription-induced DNA supercoiling. Furthermore, our data suggest that long-distance antagonistic interaction can occur not only between RNAPs from the same gene but also between RNAPs from different genes.

RESULTS

Large Variations in Promoter Strength Do Not Affect the Rate of Transcription Elongation

To examine how modulation of the initiation rate may affect the elongation rate, we used the *lac* operon of *E. coli*, a paradigm of bacterial gene regulation. The activity of the native *lac* promoter can easily be tuned by varying the concentrations of the membrane-permeable inducer isopropyl β-D-1-thiogalactopyranoside (IPTG) (Monod, 1956). This, in effect, modulates the transcription initiation rate and thus the average density of co-transcribing RNAPs on the DNA. In addition, the *lac* promoter can be rapidly shut off by the addition of glucose or orthonitrophenyl-β-D-fucoside (ONPF) (Adesnik and Levinthal, 1970). The first gene of the *lac* operon encodes LacZ, a β-galactosidase whose production can be monitored using the Miller assay (Miller, 1972). Because translation is coupled to transcription in bacteria (i.e., the first ribosome follows the RNAP; Figure S1A; Kohler et al., 2017; Landick et al., 1985; Miller et al., 1970; Proshkin et al., 2010), the apparent rate of transcription elongation, *r*, can be estimated by dividing the length of the *lacZ* transcript (3,072 nt) by the time span between IPTG addition and the rise in β-galactosidase activity (see STAR Methods; Jin et al., 1992; Kepes, 1969; Schleif et al., 1973).

In wild-type *E. coli* (MG1655) grown in M9 medium supplemented with glycerol, casamino acids, and thiamine (M9glyCaaT) at 30°C, addition of 1 or 0.2 mM IPTG resulted in maximal promoter activity while 0.1 and 0.05 mM IPTG gave rise to intermediate and low activities, respectively (Figure 1A). If close-distance cooperation occurs between RNAPs under these conditions, both push and push-pull models predict an increase in *r* with RNAP density and hence promoter activity (Epshtein and Nudler, 2003; Heberling et al., 2016). Inconsistent with this expectation, we found that the first functional LacZ enzymes appear at about the same time (~110 s) under maximal, intermediate, and low IPTG concentrations (intercept with the baseline in Figures 1B and S1B). In other words, *r* was similar ($r \approx 3{,}072/110$, ≈28 nt/s) under all tested promoter activities (Figure 1C), despite a concomitant reduction in LacZ synthesis up to 4-fold (Figure 1A).

Because inducing conditions can vary under different growth conditions, we repeated these experiments with cells grown at 37°C in MOPS EZ rich defined medium supplemented with 0.2% glucose. Under this fast-growth condition, *r* also remained similar across concentrations of IPTG (1–0.1 mM) that yielded a 4-fold difference in LacZ synthesis from maximal induction (Figures S1C and S1D). The same growth conditions were used for a genome-wide RNAP profiling study (Larson et al., 2014), showing that maximal induction of *lacZ* (1 mM IPTG) results in an RNAP density that is lower than ribosomal genes (Figure S1E). If we assume that promoter activity scales linearly with RNAP density, the 4-fold range of RNAP densities for which the transcription elongation rate of *lacZ* remains unchanged (between red and brown arrows in Figure S1E) includes RNAP densities of many genes, including genes important for cellular physiology and behavior.

Because we reached the same conclusion with two different growth conditions, we used the growth condition M9glyCaaT at 30°C for all remaining *in vivo* experiments unless stated otherwise. We verified our Miller assay observations with an independent method by specifically probing mRNA synthesis over time using two-color single-molecule fluorescence *in situ* hybridization (FISH) microscopy (see STAR Methods). In this assay, 1-kb regions at the 5′ and 3′ ends of the *lacZ* mRNA (Z5 and Z3, respectively) were visualized at 1-min intervals using different fluorescently labeled probes (Figure 1D). This method provides population-averaged kinetics of transcription elongation based on measurements from thousands of cells. The shift in time between the rise in Z5 and Z3 signals (Figure 1E) represents the time required for the first RNAPs to translocate from the 5′ to the 3′ probe regions and provides another means for calculating the apparent transcription elongation rate (Iyer et al., 2016). This FISH method has two benefits over the Miller assay: (1) it directly measures the transcription elongation rate and (2) it does not include any delay associated with IPTG action because it calculates *r* from the appearance time of two mRNA regions (Z5 and Z3). Using this FISH approach, we found that *r* was the same (~30 nt/s) under maximal (0.2 mM) and low (0.05 mM) IPTG induction conditions (Figure 1F), in good quantitative agreement with the Miller assay data (Figure 1C).

Our results indicate that modulating the rate of transcription initiation by several folds does not affect the rate of transcription

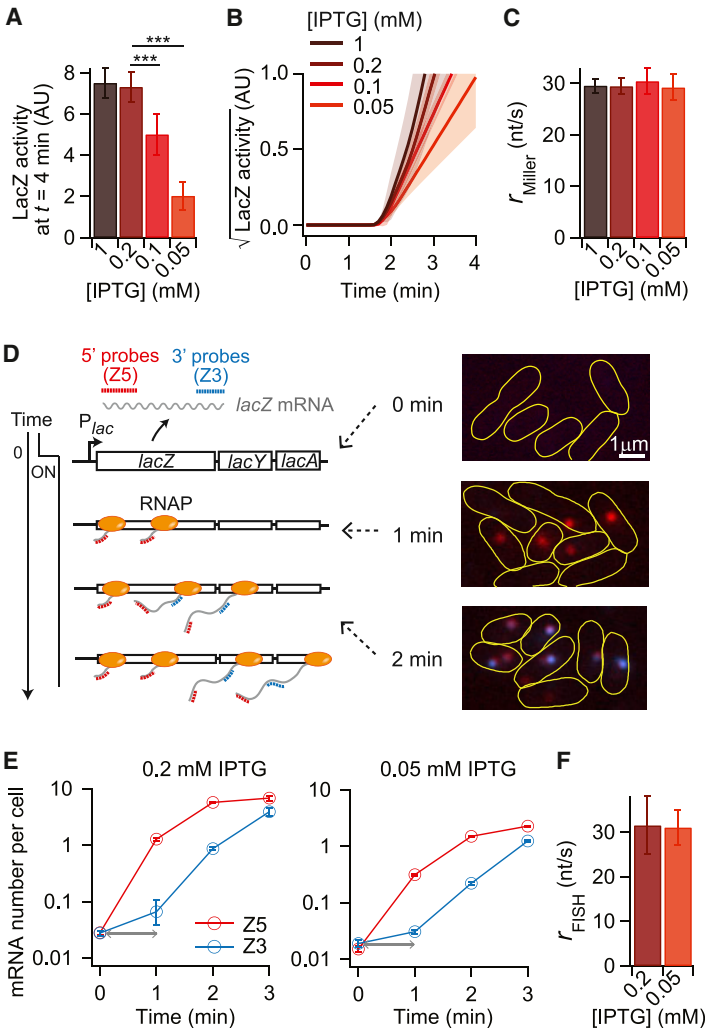

Figure 1. Effect of Promoter Strength on the Apparent Rate of Transcription Elongation

(A–F) Expression of *lacZ* in wild-type *E. coli* MG1655 cells grown at 30°C in M9glyCaaT was assayed over time by Miller assay (A–C) or single-molecule mRNA FISH microscopy (D–F) following induction with the indicated IPTG concentrations at $t = 0$ min.

(A) LacZ activity (after baseline subtraction) measured 4 min after IPTG addition (i.e., soon after the average RNAP speed measurements were made. Note that the obtained fold-changes in LacZ activity at $t = 4$ min are consistent with those obtained from steady-state measurements of mRNA copy number; So et al., 2011). *** denotes a statistically significant decrease ($p \leq 0.001$; two-sample t test). Error bars show the SD for six, eight, six, and thirteen experiments for the 1, 0.2, 0.1, and 0.05 mM IPTG conditions, respectively.

(B) Kinetics of the square root of LacZ activity following IPTG addition at $t = 0$ min. The square root was used because the LacZ amount is expected to increase as a function of t^2 (Schleif et al., 1973). Lines and shaded areas indicate the means and SDs of two-line fits (a baseline fit from $t = 0$ min to the appearance of LacZ and a linear fit of the initial increase in LacZ activity) done on each time course experiment (example traces are shown in Figure S1B). The number of experiments is noted in (A).

(C) Apparent transcription elongation rate of *lacZ* at indicated IPTG concentrations. Error bars show SDs.

(D) Schematic and representative images of single-molecule two-color FISH microscopy experiments used to measure *lacZ* mRNA levels over time. Red and blue dotted lines indicate Cy5 or Cy3B fluorescently labeled oligonucleotide probes that hybridize to 1-kb-long 5′ (Z5) and 3′ (Z3) mRNA regions of *lacZ*, respectively. Also shown are overlays of two fluorescence images with pseudo-coloring for Cy5 (red) and Cy3B (blue) at indicated time points after IPTG addition. Data shown at $t = 0$ min are from a sample collected before IPTG addition.

(E) Z5 and Z3 mRNA numbers per cell over time after IPTG addition at $t = 0$ min. The gray arrows show the time shift in Z3 mRNA appearance (STAR Methods). Error bars are bootstrapped SEMs. At least 1,200 cells were analyzed per time point.

(F) Effect of different promoter activities on the apparent transcription elongation rate of *lacZ*, calculated by dividing the distance between the two probe regions (2,000 nt) by the time shift between the Z5 and Z3 mRNA signals. Error bars are SDs of five and eight experiments for the 0.2 and 0.05 mM IPTG conditions, respectively.

See also Figure S1.

elongation. This suggests that the RNAP density produced by the fully induced *lac* promoter is not sufficient to produce a cumulated RNAP push or push-pull effect large enough to significantly alter the apparent rate of elongation.

Turning Off an Active Promoter Results in Apparent Slowdown of Transcribing RNAPs

A straightforward interpretation for the lack of correlation between promoter activity and transcription elongation rate is that RNAPs do not affect each other's motion under the tested range of RNAP densities. If this was true, turning off an active promoter—a common natural occurrence in response to environmental changes—should not have any effect on the apparent elongation rate of already-loaded RNAPs. To our surprise, this is not what we observed. Because the Miller and FISH assays report on the elongation rate of the first loaded RNAPs after IPTG induction, we shut off the promoter before the first RNAPs reached the end of the *lacZ* gene by adding an anti-inducer, ONPF or glucose, 90 s after addition of 0.2 mM (maximal) or 0.05 mM (low) IPTG. At both IPTG concentrations, LacZ synthesis was significantly delayed following promoter repression (Figures 2A and S2A–S2D). For example, under the condition of 0.2 mM IPTG, we detected functional LacZ only at $t \approx 175$ s, compared to $t \approx 110$ s when the promoter remained active. Because the conditions were the same for the first 90 s, these results imply that it took more than four times longer (175 s − 90 s = 85 s versus 110 s − 90 s = 20 s) for the first RNAPs to complete *lacZ* transcription following promoter repression (Figure 2B). Thus, the average speed of the leading RNAPs after promoter repression (r_{OFF}) was about 4-fold lower than when the promoter remains active (r_{ON}; Figure 2C). We note that considering RNAP pause sites over the *lacZ* DNA template (Larson et al., 2014; Figures S2E and S2F) or not produced similar results and conclusions (Figure 2C versus S2G). Therefore, we ignored pause sites from r_{OFF} calculations hereafter.

The decrease in average RNAP speed following promoter repression is remarkable because the first RNAPs are over 2 kb downstream of the promoter (based on their average elongation rate) when the anti-inducer is added, indicating that the state of the promoter (active versus repressed) has a long-distance effect on already-transcribing RNAPs. A decrease in *r*

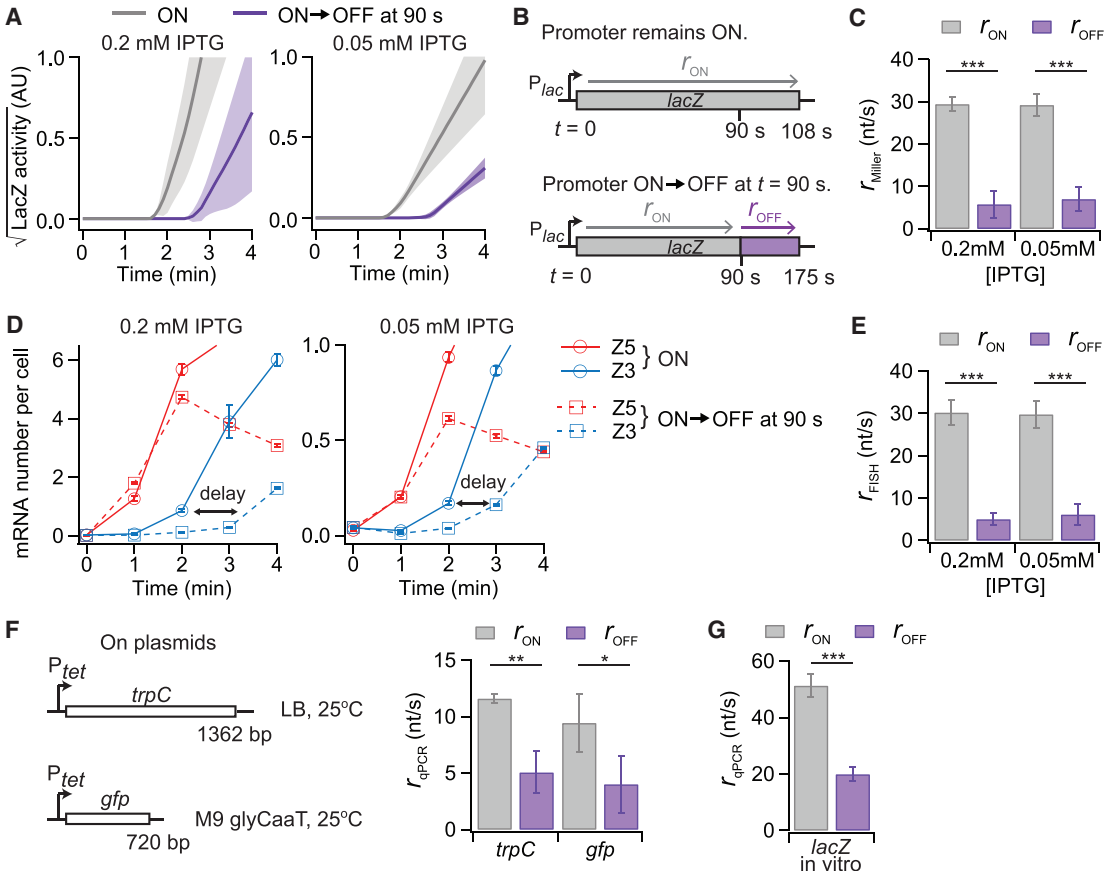

Figure 2. Effect of Promoter Repression on the Transcription Elongation Rate

(A) Miller assay results showing the kinetics of the square root of LacZ activity for wild-type *E. coli* MG1655 cells grown in M9glyCaaT at 30°C, depending on whether the promoter remains induced (ON) or is turned off (ON → OFF). The promoter was repressed by addition of 5 mM ONPF or 500 mM glucose at t = 90 s after induction with 0.05 or 0.2 mM IPTG, respectively. Lines and shaded areas indicate the means and SDs of two-line fits on each time course trace (n = 8 [ON] and 6 [ON → OFF] experiments for 0.2 mM IPTG condition and n = 13 [ON] and 11 [ON → OFF] experiments for the 0.05 mM IPTG condition).

(B) Schematics defining r_{ON} versus r_{OFF} as the average speed of the first RNAPs when the promoter is active versus when it is turned off at t = 90 s. Shown are the time results for the 0.2 mM IPTG condition in (A). See STAR Methods for a detailed description of how r_{OFF} was calculated.

(C) Effect of promoter inactivation on r measured by the Miller assay. ***p ≤ 0.001 (two-sample t test). Error bars were calculated based on SDs of replicates described in (A) and propagation of error in r_{OFF} calculation (see STAR Methods).

(D) Z5 and Z3 mRNA numbers per cell over time in FISH microscopy experiments in which the promoter remained active or was turned off by addition of 500 mM glucose at t = 90 s. Black arrows indicate the delay in Z3 signal appearance from the basal level in the promoter-repression case. Over 1,200 cells were analyzed per time point. Error bars are bootstrapped SEMs.

(E) Effect of promoter repression on r measured by two-color mRNA FISH microscopy shown in (D). Error bars are based on SDs of n > 4 experiments and propagation of error in r_{OFF} calculation (see STAR Methods). ***p ≤ 0.001 (two-sample t test).

(F) Effect of promoter repression on r for indicated genes of different lengths driven by a synthetic promoter P_{tet}, as measured by quantitative real-time PCR. After induction with 100 ng/mL aTc, the expression of *trpC* or *gfp* was repressed by adding 400 μg/mL rifampicin at t = 75 (*trpC*) or 60 s (*gfp*). **p ≤ 0.01 and *p ≤ 0.05 (two-sample t test). Error bars are based on SDs of three experiments and propagation of error in r_{OFF} calculation.

(G) Apparent transcription elongation rate of *lacZ* measured *in vitro* using a plasmid containing *lacZYA* driven by the *lac*UV5 promoter. At t = 0 s, purified *E. coli* RNAP holoenzyme was added to induce multi-round transcription. At t = 30 s, 400 μg/mL rifampicin was added for promoter repression. Error bars are based on SDs of n > 6 experiments and propagation of error in r_{OFF} calculation. ***p ≤ 0.001 (two-sample t test).

See also Figures S2 and S3.

was also observed when the promoter was turned off with rifampicin (Figure S3A), which blocks RNAPs at the promoter but not during transcription elongation (Campbell et al., 2001; McClure and Cech, 1978; Mosteller and Yanofsky, 1970).

One possible explanation could be that promoter inactivation somehow caused the formation of a long-lived pause near the end of the *lacZ* gene, slowing down the first RNAPs. In such a case, shutting off the promoter earlier (e.g., t = 45 s instead of t = 90 s) would result in the same delay, as the RNAPs should only experience this pause when they encounter it. Instead, we found that turning off the promoter at t = 45 s resulted in even further delay in the first appearance of LacZ activity (Figure S3B), suggesting that the earlier the promoter is repressed, the longer it takes for the first RNAPs to complete *lacZ* transcription.

This observation argues that RNAPs slow down immediately after the promoter is turned off.

We confirmed the long-distance effect of promoter repression on transcription elongation using FISH microscopy experiments in which the promoter either remained active or was turned off with glucose 90 s after addition of 0.2 mM IPTG. The Z5 mRNA signal appeared at the 1-min time point in both cases (Figure 2D), which was expected, as it occurred before glucose addition. However, the first appearance of the Z3 mRNA signal was delayed from the 2-min time point to the 3-min time point when the promoter was shut off compared to when it remained active (Figure 2D). This delay reflects a reduction in apparent RNAP speed following promoter repression (Figure 2E), in agreement with the Miller assay results (Figure 2C). We obtained similar results with 0.05 mM IPTG (Figures 2D, 2E, and S3C), despite the expected lower RNAP density on the DNA template.

These observations were recapitulated in a Δ*lacYA* strain (Figure S3D), thereby ruling out any potential effect from the expression of downstream genes *lacY* and *lacA* (e.g., LacY-dependent positive feedback on transcription initiation [Novick and Weiner, 1957; Ozbudak et al., 2004]). The delay in *lacZ* transcription upon promoter repression was also independent of the genomic context, as it was reproduced in a strain in which the *lac* operon is expressed from a plasmid instead of its native chromosomal locus (Figure S3E). Moreover, we also observed an apparent RNAP slowdown in response to promoter repression for two different genes, *trpC* and *gfp* (Figures 2F, S3F, and S3G). In these experiments, *trpC* and *gfp* were plasmid encoded and expressed from the anhydrotetracycline (aTc)-inducible promoter (P_{tet}). We measured the rate of transcription elongation by probing 5′ and 3′ regions of the transcripts by quantitative real-time PCR (qPCR) after adding aTc at $t = 0$ min (STAR Methods). As *trpC* (1.36 kb) and *gfp* (0.72 kb) are considerably shorter in length than *lacZ* (3.07 kb), we grew the strains and performed the assay at 25°C. This lower temperature sufficiently reduced the transcription kinetics for us to confidently measure the time delay between 5′ and 3′ end probe signals and to block promoter activity with rifampicin before the first RNAPs finish transcription. In the case of the plasmid-encoded *trpC*, we used Luria-Bertani medium (LB, which contains tryptophan) instead of M9glyCaaT to prevent transcription of the endogenous chromosomally encoded *trpC* gene. Our results indicate that the negative effect of promoter repression on the speed of promoter-distal RNAPs is robust to differences in gene sequence, gene length, promoter, growth medium, and temperature. This is therefore likely to be a general phenomenon.

The Apparent RNAP Slowdown in Response to Promoter Repression Occurs *In Vitro* with the Minimal Set of Components Needed for Transcription

To examine whether our promoter-repression observations are linked to an inherent property of transcription (i.e., independent of other cellular processes), we turned to an *in vitro* transcription assay. For this, we used a plasmid containing the original *lac* operon sequence with a two-base mutation in the promoter (*lac*UV5), which is commonly used in *in vitro* studies because it does not require a Catabolite Activator Protein (CAP) for full promoter activity (Noel and Reznikoff, 2000). Because transcription is independent of IPTG *in vitro* (no LacI repressor), expression from the *lac*UV5 promoter was induced by adding purified *E. coli* RNAPs to the reactions. We found that shutting off the promoter with rifampicin before the first RNAPs completed *lacZ* transcription significantly reduced their apparent speed *in vitro* (Figure 2G), despite the absence of ribosomes or cellular factors other than RNAPs and the plasmid template. This suggests that the reduced rate of transcription elongation observed *in vivo* results from an intrinsic property of transcription.

The Negative Effect of Promoter Repression on Transcription Elongation Involves Transcription-Induced DNA Supercoiling

How can shutting off a promoter rapidly affect the translocation of RNAPs that are >2 kb away from the promoter? We hypothesized that the apparent slowdown of transcription elongation after promoter repression may be related to DNA supercoiling that is intrinsically generated by RNAPs when they translocate on a topologically constrained DNA template (i.e., cannot easily rotate). During transcription, individual RNAPs generate negative DNA supercoiling upstream and positive DNA supercoiling downstream (Liu and Wang, 1987). On the other hand, single-molecule *in vitro* experiments have shown that accumulation of negative DNA supercoils upstream of an RNAP inhibits the translocation of this polymerase due to torsional stress (Ma et al., 2013). We reasoned that, when two RNAPs transcribe the same DNA template, negative and positive DNA supercoils between RNAPs may cancel out (Figure 3A), as previously hypothesized (Guptasarma, 1996; Koster et al., 2010; Liu and Wang, 1987). Therefore, we envisioned that DNA supercoil cancellation by neighboring RNAPs prevents the accumulation of negative DNA supercoils and reduces torsional stress, promoting a more "fluid" mode of transcription elongation (Figure 3A). In this working model, DNA supercoil cancellation also occurs between distantly spaced polymerases (i.e., at low RNAP density). This is conceivable, as DNA supercoils can diffuse (van Loenhout et al., 2012). In our model, sustained loading of RNAPs (i.e., no promoter repression) is important, as it ensures that the level of negative DNA supercoiling behind the last-loaded RNAP (i.e., the one closest to the promoter) does not accumulate beyond an inhibitory threshold.

Such a fluid mode of transcription elongation would be abrogated when the loading of new RNAPs stops (i.e., when the promoter becomes repressed). Accumulation of negative DNA supercoils behind the last-loaded RNAP would cause it to slow down or stall (Figure 3A). This slower RNAP would then generate fewer positive DNA supercoils downstream, reducing its long-distance assistance on the translocation of the nearest downstream RNAP through DNA supercoil cancellation. A slowdown or stalling of this downstream RNAP would then have the same negative effect on the translocation of the next RNAP and so forth (Figure 3A). As a result, the disruptive torsional effect on the translocation of the last-loaded RNAP would rapidly propagate to RNAPs far downstream, creating a "torsionally stressed" mode of elongation (Figure 3A).

This model predicts that reducing torsional stress from accumulated negative DNA supercoils should restore normal RNAP speed after promoter inactivation. Consistent with this

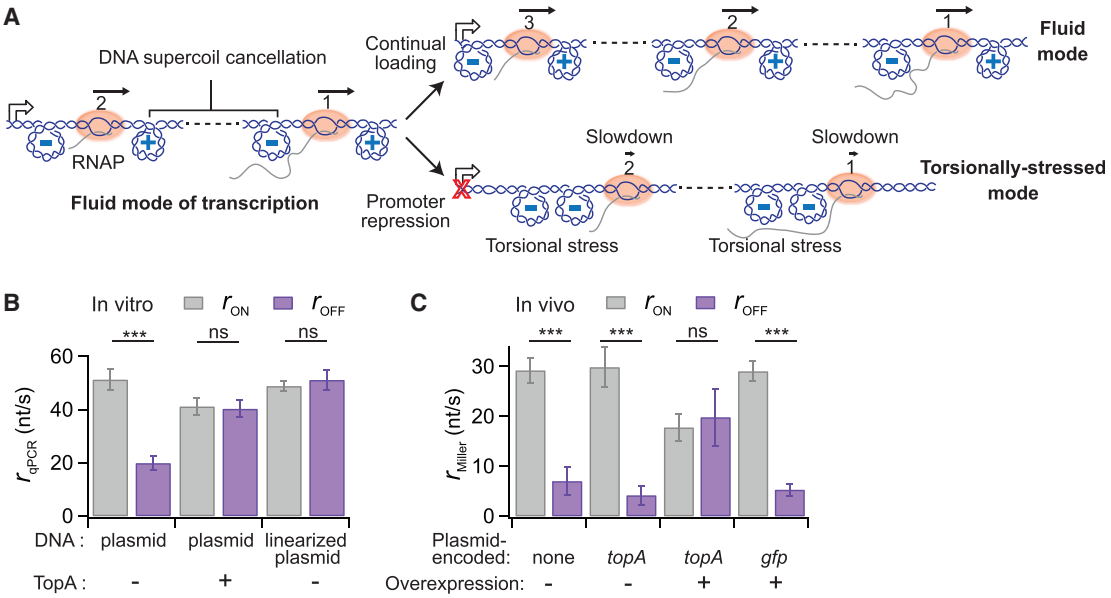

Figure 3. Effect of DNA Supercoiling on *lacZ* Transcription Kinetics Depending on the Active or Repressed State of the Promoter

(A) Schematic showing the proposed model for transcription-driven DNA supercoiling affecting RNAP kinetics, depending on whether the promoter remains active or becomes repressed. See text for details.

(B) Effect of TopA activity and plasmid linearization on the apparent rate of transcription elongation of *lacZ in vitro*. Same *in vitro* transcription experiments as in Figure 2G are shown except that two conditions were added for comparison: in the presence of TopA or using the same plasmid as template but after its linearization. Error bars are based on SDs of four experiments for each condition and propagation of error in r_{OFF} calculation. ***p $\leq$ 0.001 (two-sample t test), and ns indicates a statistically non-significant difference.

(C) Effect of TopA overproduction on the apparent rate of transcription elongation of *lacZ in vivo*. P_{lac} was turned on with 0.05 mM IPTG at t = 0 s and repressed by 5 mM ONPF at t = 90 s. The *topA* gene was encoded on the plasmid as a second copy under P_{tet} (strain CJW6920), and its overexpression was induced with 100 ng/mL aTc 15 min before addition of 0.05 mM IPTG (this induction condition was selected based on the results shown in Figure S4). For comparison, we present data from MG1655 cells (no plasmid), CJW6920 cells without aTc (plasmid present but no induction of *topA* overexpression), and CJW6919 cells overexpressing *gfp* (instead of *topA*) from the same plasmid and promoter by addition of 100 ng/mL aTc for 15 min prior to IPTG addition. Error bars are based on SDs of at least three experiments for each condition and propagation of error in r_{OFF} calculation. ***p $\leq$ 0.001 (two-sample t test), and ns indicates a statistically non-significant difference.

See also Figure S4.

prediction, adding type I topoisomerase (TopA) to the *in vitro* transcription reaction in order to remove negative DNA supercoils resulted in similar average elongation rates, regardless of whether the promoter remained active or was turned off by rifampicin (Figure 3B). We note that the elongation rate with the active promoter (no rifampicin) was lower in the presence of TopA than in its absence. One possible explanation is that TopA not only removes the accumulated negative DNA supercoils behind the last RNAP when the promoter is turned off but also removes negative DNA supercoils in between RNAPs before they can cancel out with positive DNA supercoils. An accumulation of positive DNA supercoils can also impact RNAP translocation (Chong et al., 2014; Ma et al., 2013; Rovinskiy et al., 2012), which could potentially explain the lower r value in the presence of TopA. To reduce accumulation of any type of DNA supercoils, we linearized the plasmid, allowing DNA supercoils to dissipate at the free ends. Linearization of the DNA template both restored the higher rate of transcription elongation and abrogated any effect that repressing the promoter had on the elongation rate (Figure 3B). These results indicate that transcription-induced DNA supercoiling mediates the change in elongation dynamics in response to promoter repression.

We hypothesized that, inside cells, the supply of TopA may be insufficient to respond to a quick accumulation of negative DNA supercoils in a timely fashion. If that was the case, a brief overexpression of TopA may prevent the negative effect of promoter repression on transcription elongation. Consistent with the *in vitro* observations (Figure 3B), overexpression of plasmid-encoded *topA* for 15 min from the aTc-inducible P_{tet} decreased r_{ON} (Figure 3C). More importantly, *topA* overexpression abrogated the negative promoter-repression effect, as r_{OFF} remained similar to r_{ON} after addition of the anti-inducer (Figure 3C), supporting our hypothesis. As a control, we showed that overexpression of *gfp* under the same conditions had no effect (Figures 3C and S4).

A Solo RNAP Displays a Slower Apparent Speed Than Multiple Co-transcribing RNAPs and Is Not Affected by Promoter Repression

According to our model, if there is only a single RNAP per template, as expected for repressed or weakly expressed genes at steady state, the absence of torsional stress relief from co-transcribing RNAPs through DNA supercoiling cancellation should result in a reduced transcription elongation rate. This is, indeed,

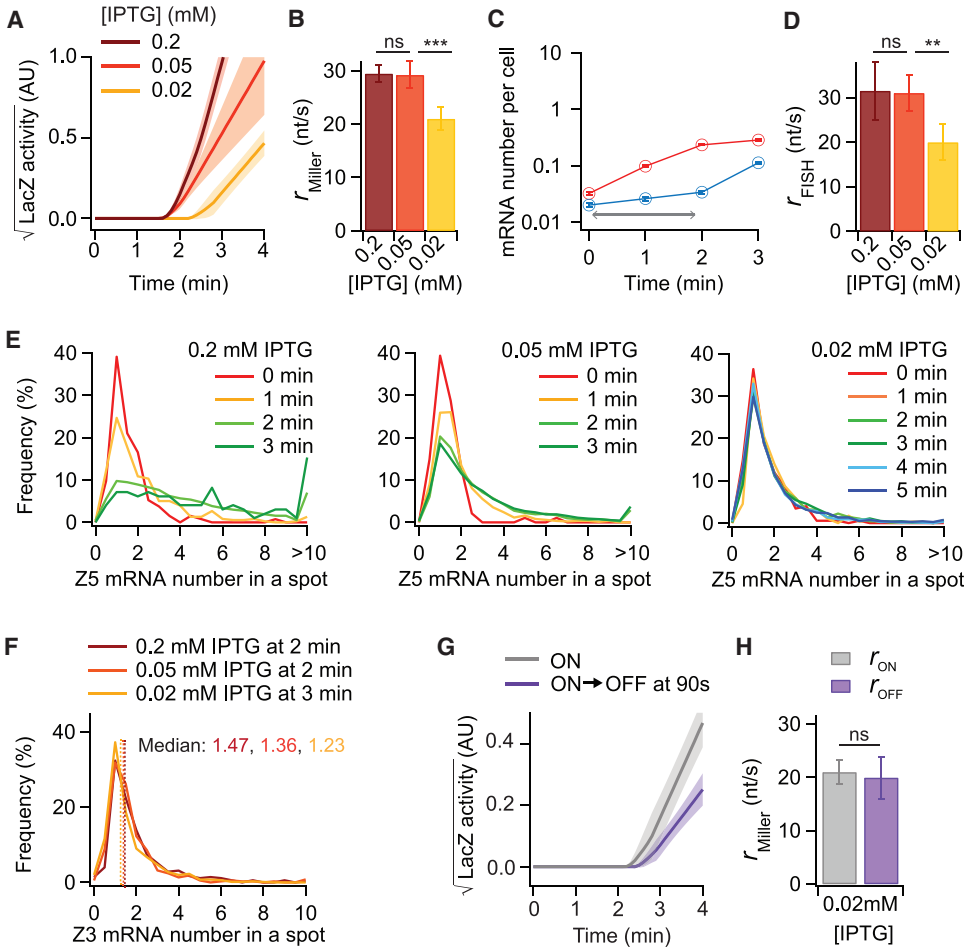

Figure 4. Transcription Elongation Kinetics when the *lac* Promoter Is Minimally Induced

(A) Kinetics of the square root of LacZ activity in wild-type *E. coli* MG1655 cells (grown in M9glyCaaT at 30°C) following addition of IPTG at the indicated concentrations. Lines and shaded areas indicate the means and SDs of two-line fits on each time course trace from at least three experiments.

(B) Apparent transcription elongation rate of *lacZ* at indicated IPTG concentrations. Error bars show SDs of at least three experiments. ***$p \leq 0.001$ (two-sample t test), and ns indicates a statistically non-significant difference.

(C) Evolution of Z5 and Z3 mRNA numbers per cell after 0.02 mM IPTG addition. The gray arrow shows the time shift between the Z5 and Z3 signal appearance. Error bars are bootstrapped SEMs. At least 7,000 cells were analyzed per time point.

(D) Effect of different induction levels of *lacZ* expression on the apparent transcription elongation rate, as calculated from FISH data. Error bars are SDs of at least three experiments. **$p \leq 0.01$ (two-sample t test), and ns indicates a non-significant difference.

(E) Distribution of Z5 mRNA numbers in a fluorescent spot inside cells at each time point for different IPTG concentrations (n = 400–2,000 spots for each time point).

(F) Distribution of Z3 mRNA numbers in a fluorescent spot at indicated time points for different IPTG concentrations. At these time points, the first RNAPs complete or have just completed transcription of the first gene (*lacZ*) of the *lac* operon (n = 300–1,000 spots for each condition).

(G) Kinetics of the square root of LacZ activity when the promoter remained active (n = 5 experiments) or was turned off (n = 3 experiments) 90 s after induction with 0.02 mM IPTG. Lines and shaded areas respectively indicate the means and SDs of two-line fits on each time course trace.

(H) Apparent transcription elongation rate of *lacZ* under conditions described in (G). Error bars are based on SDs of replicates and propagation of error in r_{OFF} calculation. ns indicates a non-significant difference (p = 0.54 based on a two-tailed t test).

See also Figure S5.

what we observed in Miller assays when *lacZ* expression was induced with only 0.02 mM IPTG (Figures 4A and 4B). We obtained the same result of reduced *r* from FISH experiments, whether we considered all cells (Figures 4C and 4D) or only cells with mRNA signal (Figure S5A). Under this very low induction condition, only a single RNAP was present on the *lacZ* template, based on the observation that the number of Z5 mRNAs per fluorescent spot did not increase over time following IPTG induction, unlike at higher IPTG concentrations (Figure 4E). At 0.02 mM IPTG, the number of Z5 mRNAs per spot remained near 1, similar to the repressed state ($t = 0$ min); only the number of cells with Z5 spots increased over time following IPTG induction (Figure S5B).

Our FISH data can also inform on the clustering of RNAPs (or lack thereof) by examining the number of Z3 mRNAs per

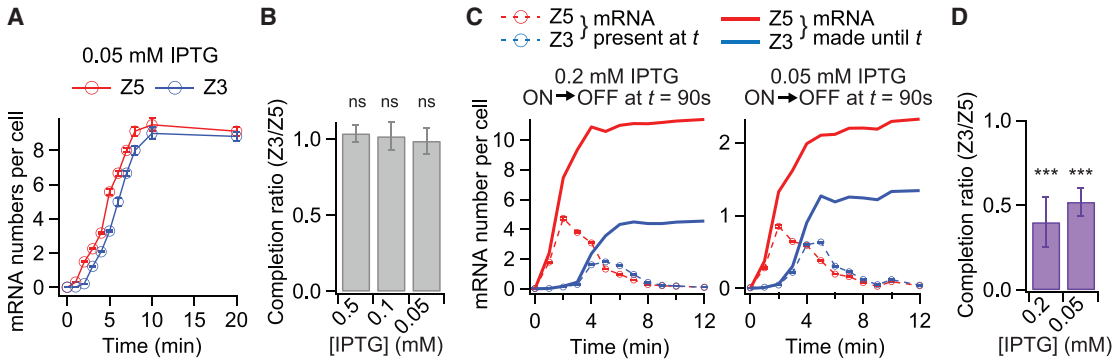

Figure 5. Premature Dissociation of Already-Loaded RNAPs following Promoter Repression

We estimated the fraction of RNAPs that made Z5 mRNA and reached the Z3 mRNA region by examining the amount of Z5 and Z3 mRNA synthesis at the end of the time course experiments, using wild-type *E. coli* MG1655 cells grown in M9glyCaaT at 30°C.

(A) Temporal change in the mean Z5 and Z3 mRNA numbers per cell under continuous induction of *lacZ* expression with 0.05 mM IPTG (promoter remains active). Over 1,500 cells were analyzed per time point. Error bars are bootstrapped SEMs.

(B) Transcription completion ratio, i.e., ratio of RNAPs completing *lacZ* transcription in (A), calculated by dividing the Z3 plateau level by that of Z5. Over 7,500 cells were analyzed for each IPTG concentration. Error bars are SDs of four, four, and five experiments for the 0.5, 0.1, and 0.05 mM IPTG conditions, respectively. A statistically non-significant difference to 1 (one-sample t test) is indicated by ns.

(C) Accumulation of Z5 and Z3 mRNA numbers per cell when the promoter is turned off at $t = 90$ s. The total number of Z5 and Z3 mRNAs made until each time point (solid line) was calculated from their FISH signals (circles and dotted lines) using Equation 7 (see STAR Methods). Over 2,000 cells were analyzed per time point. Error bars are bootstrapped SEMs.

(D) Transcription completion ratio, calculated from (C) by dividing the plateau level of Z3 by that of Z5. Error bars are SDs of four and six experiments for the 0.2 and 0.05 mM IPTG conditions, respectively. *** indicates a statistically significant difference to 1 ($p \leq 0.001$; one-sample t test).

See also Figure S6.

fluorescent spots at a time point at which the first RNAPs complete or have just completed transcription of the first gene (*lacZ*) of the *lac* operon ($t = 2$ min for 0.2 and 0.05 mM IPTG and $t = 3$ min for 0.02 mM IPTG). If multiple RNAPs were closely spaced during elongation (traveling as convoys), they would transcribe the last 1,000-bp DNA region of *lacZ* (corresponding to the Z3 mRNA) at the same time. In such a case, we should observe multiple Z3 mRNAs produced from the same gene (i.e., from the same fluorescent spot). The number of Z3 mRNAs would scale with the number of RNAPs within the convoy. If, in contrast, RNAPs were sparsely distributed and traveled at distance from each other (no RNAP convoy), only one or two RNAPs would transcribe the 1-kb Z3 region at the same time. In this case, we should observe less than two Z3 mRNAs per fluorescent spot. We observed the latter under all IPTG conditions tested (Figure 4F). Even when *lacZ* was maximally induced with 0.2 mM IPTG (Figure 4F), the median value of Z3 mRNA per fluorescent spot was only 1.47. This argues against the prevalence of RNAP convoys under our experimental conditions.

The slower elongation rate under the 0.02 mM IPTG condition (Figures 4B and 4D) demonstrates that a single RNAP behaves differently than multiple RNAPs when the promoter remains active. A single RNAP was also largely insensitive to promoter repression, as we did not observe a significant delay in LacZ activity appearance when the *lac* promoter was turned off 90 s after addition of 0.02 mM IPTG (Figures 4G, S5C, and S5D), resulting in $r_{OFF} \approx r_{ON}$ (Figure 4H). Thus, the apparent slowdown in transcription elongation when the promoter is turned off is not a property of a single RNAP; instead, it is an emergent property of multiple RNAPs transcribing the same DNA.

Promoter Repression Promotes Premature Transcription Termination

A significantly lower rate of transcription elongation often means longer or more frequent RNAP pauses and more efficient transcription termination (Fisher and Yanofsky, 1983; Guarente and Beckwith, 1978; Jin et al., 1992; Kotlajich et al., 2015; McDowell et al., 1994; Peters et al., 2011; Yanofsky and Horn, 1981). Furthermore, a mutation in RNAP that reduces elongation rate in yeast reduces processivity (Mason and Struhl, 2005). Thus, a potential functional consequence of RNAP slowdown following the repression of an active promoter may be an increase in premature transcription termination. Time course analysis of the *in vivo* FISH data revealed that, under continuous induction, the Z5 and Z3 signals reached a similar plateau at steady state (Figure 5A), leading to a Z3/Z5 signal ratio close to 1 for different (0.05–0.5 mM) IPTG concentrations (Figure 5B). Because the degradation rates of the Z3 and Z5 regions were the same (with a mean lifetime of ~1.5 min; Figure S6B), these results indicate that premature termination during *lacZ* transcription is negligible when the promoter remains active, as previously reported (Iyer et al., 2016). In contrast, when the promoter was shut off at 90 s, only ~50% of the RNAPs that transcribed the Z5 probe region reached the Z3 region (Figures 5C and 5D). Thus, a reduced elongation rate in response to a block in transcription initiation is accompanied with a significant increase in premature dissociation of the already-loaded RNAPs.

Analysis of our *in vitro* data confirmed that this negative effect of promoter repression on RNAP processivity is due to transcription-induced torsional stress, as the completion ratio between 5′ end and 3′ end mRNA regions increased from 0.33 to either 0.87 when TopA was added to the reaction or 1.00 when the linearized

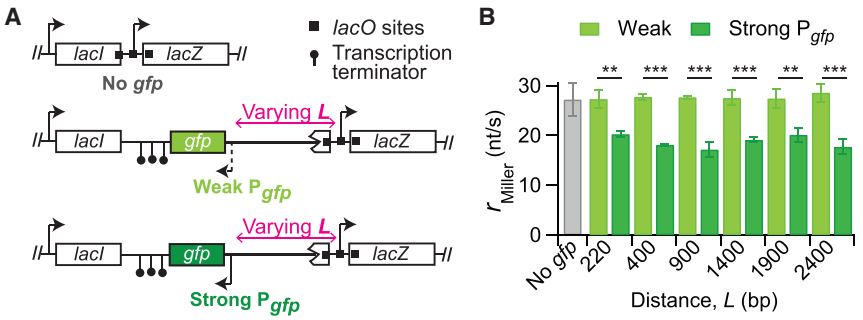

Figure 6. Effect of Transcription of a Divergently Transcribed Gene on Transcription Elongation of the *lacZ* Gene

(A) Schematics of constructs used to test the effect of upstream divergent gene activity on transcription elongation of *lacZ* (not drawn to scale). The transcription start sites of the *lacZ* and *gfp* genes were separated by a DNA varying in length (*L*) from 220 to 2,400 bp.

(B) Apparent transcription elongation rate of *lacZ* for different constructs, as measured by the Miller assay under 0.2 mM IPTG induction when cells were grown in M9glyCaaT at 30°C (as in Figure 1C). Error bars show SDs of at least three experiments. $^{**}p \leq 0.01$ and $^{***}p \leq 0.001$ (two-sample t test). See also Figure S7.

plasmid was used (Figures S6D and S6E). Thus, a reduced elongation rate in response to a block in transcription initiation is associated with a significant increase in premature dissociation of the already-loaded RNAPs. For polycistronic genes, such as the *lac* operon, this premature transcription termination also suppresses the expression of downstream genes. In nature, where bacteria experience rapidly changing environments, this outcome would be particularly advantageous, as it provides a means for cells to more quickly stop the production of unneeded mRNAs and thus proteins when the inducing conditions disappear.

Expression from a Gene Can Impact the Transcription Elongation Rate of a Divergently Transcribed Gene

So far, we have considered intragene effects involving RNAPs on the same DNA template. According to our proposed mechanism, negative DNA supercoiling created by RNAP translocation on a gene may also reduce the speed of RNAPs on a neighboring divergently oriented gene, as transcription-generated DNA supercoils have been observed to spread far (>2 kb) away from the transcription sites (Kouzine et al., 2013; Naughton et al., 2013a; Wang and Dröge, 1997).

To test this prediction, we inserted *gfp*, driven by either a strong or a weak promoter, between *lacI* and *lacZ* on a plasmid in the Δ*lacZYA* strain (Figure 6A). Both promoters were derived from the *E. coli ompA* promoter, which we mutated to modulate its strength (Figure S7). Consistent with our model prediction, *gfp* expression from the strong promoter reduced the apparent transcription elongation rate of *lacZ* when its expression was induced with 0.2 mM IPTG (Figure 6B). This antagonistic effect was observed even when the *gfp* and *lacZ* transcription start sites were separated by as much as 2,400 bp (Figure 6B). Thus, long-distance antagonistic dynamics can also emerge from RNAPs transcribing separate genes.

DISCUSSION

In this study, we show that RNAPs display emergent group behaviors over long distances. Here, we define an RNAP group as multiple RNAPs transcribing a DNA template at the same time, regardless of their spacing. Our definition of group is based on affiliation rather than close proximity. In this context, an RNAP group can, but does not have to, involve RNAP convoys. In fact, our data suggest that RNAPs do not form convoys under our experimental conditions (Figure 4F). Although our approach does not directly examine the number of RNAPs per DNA template, the Z5 mRNA number per Z5- and Z3-colocalized spot when the first RNAPs have just completed *lacZ* transcription is related to RNAP density (Figure S5E), as Z5 mRNA degradation is negligible by $t = 2$ min (Figure 5C). At low IPTG concentration (0.05 mM), we observed the same apparent elongation rate and the same promoter-repression effect as under maximal IPTG induction conditions (Figures 1 and 2). Yet, under 0.05 mM IPTG, the median of Z5 mRNA number per Z5- and Z3-colocalized spot at the relevant time point ($t = 2$ min) is only 3.2 (Figure S5F). This number, together with the absence of evidence for convoy formation (Figure 4F), suggests that group dynamics occurs even when very few RNAPs are sparsely distributed over the 3-kb *lacZ* template.

Our data suggest that such long-distance RNAP group behaviors emerge from three features associated with transcription on topologically constrained DNA: (1) the translocation of an RNAP generates DNA supercoiling (Liu and Wang, 1987); (2) negative DNA supercoiling impedes the motion of individual RNAPs (Ma et al., 2013); and (3) DNA supercoils are dynamic (Crut et al., 2007; Forte et al., 2019; Ganji et al., 2016; Ivenso and Lillian, 2016; Nelson, 1999; van Loenhout et al., 2012). These three features lead to either collaborative or antagonistic effects between well-separated RNAPs, depending on whether the promoter remains active or become repressed.

Collectively, our results are consistent with the following model. When the promoter remains active, the presence of multiple RNAPs on a DNA template results in fluid RNAP translocation. DNA supercoils created by the translocation of each RNAP are rapidly cancelled out between RNAPs, relieving torsional stress on these RNAPs and leading to fast and processive translocation (Figure 7A). This long-distance assistance is not additive; it is independent of RNAP density as long as positive and negative DNA supercoils between RNAPs can move toward each other and cancel out. This proposed fluid mode of transcription elongation explains why the apparent rates of transcription elongation remain similar across a significant range of promoter activities (Figures 1 and S1) and hence RNAP densities. This range of promoter activities likely covers a wide range of physiologically relevant levels of gene expression (Figure S1E). We therefore anticipate that most genes important for cellular physiology will experience a fluid mode of transcription, unlike

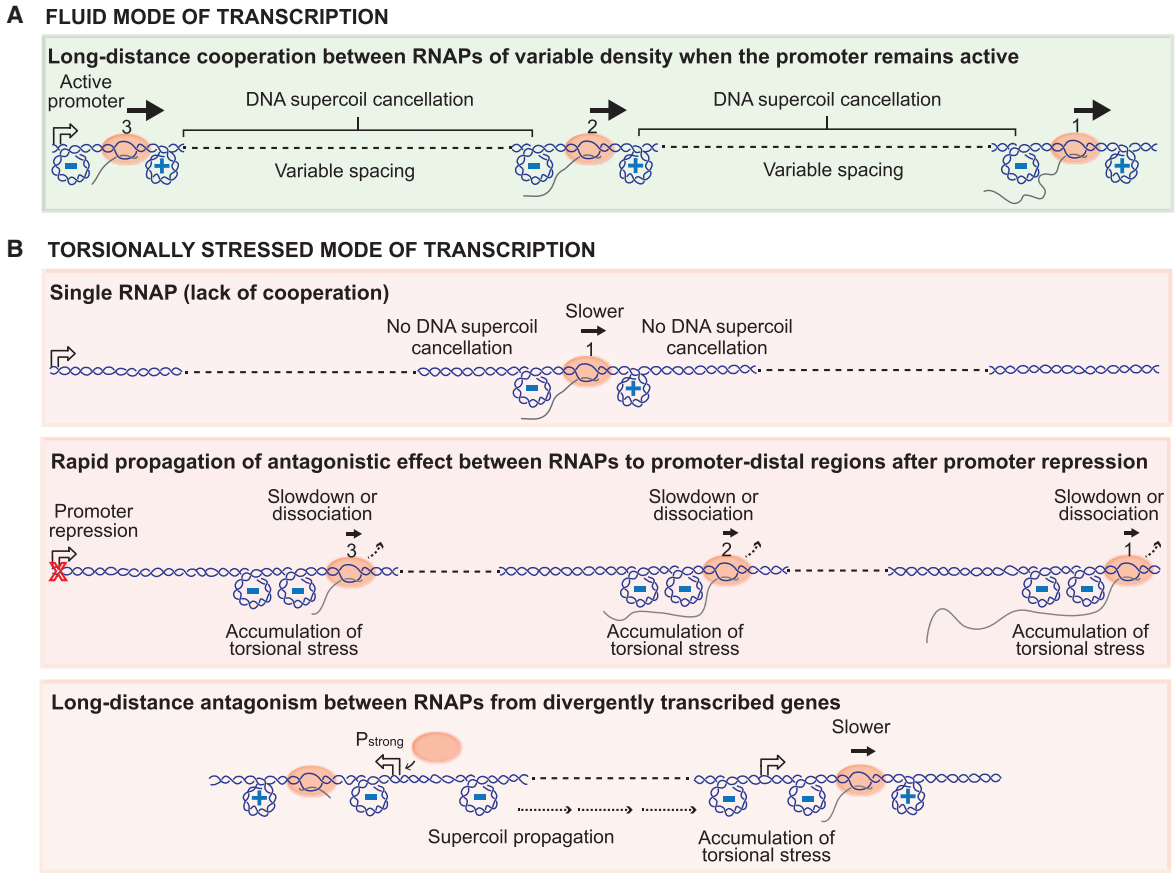

Figure 7. DNA Supercoiling on Transcription Elongation

(A) Fluid mode of transcription. See Discussion for details.

(B) Three cases of torsionally stressed mode of transcription. See Discussion for details.

repressed or poorly expressed genes that are only occasionally transcribed by a single RNAP.

In our model, long-distance assistance between RNAPs disappears when a single RNAP is transcribing (Figure 7B) or when an active promoter shuts off, because torsional stress is no longer relieved by DNA supercoiling cancellation (Figure 7B). This results in slower apparent elongation rates (Figures 2, 4, S2, S3, and S5). In the case of promoter repression, the negative effect associated with the slowdown of the promoter-proximal RNAP is quickly propagated to the downstream RNAPs (Figure 7B), as each RNAP benefits from the motion of the upstream RNAP for torsional stress relief. In fact, the most downstream RNAPs (the farthest away from the promoter) may be most sensitive to increased DNA supercoiling, as they have longer transcripts (and more ribosomes), causing higher rotational friction (Nelson, 1999; Tsao et al., 1989).

It is important to note that promoter repression results in considerably slower apparent elongation rates (Figures 2C and 2E) than what we measured for a single RNAP (Figures 4B and 4D). This suggests that, upon promoter repression, RNAPs on the same template do not just stop assisting each other; they switch their behavior from collaborative to antagonistic. How could this be possible? We speculate that this is again linked to the dynamic property of DNA supercoils. Transcribing RNAPs form complexes with nascent transcripts and associated ribosomes. These bulky complexes likely act as barriers to DNA supercoiling propagation (Booker et al., 2010; Leng et al., 2011). Therefore, DNA supercoils created between RNAPs likely remain more spatially confined compared to those created by a single RNAP. In other words, the torsional stress experienced by RNAPs within a group after promoter inactivation may be higher than that experienced by an RNAP transcribing the gene by itself. Furthermore, spatial confinement of DNA supercoiling may increase bending stress due to the formation of a plectoneme (a loop of helices twisted together), affecting RNAP speed. Consistent with this notion, critical torque for plectoneme formation is more rapidly achieved (i.e., at a lower number of twists) on shorter DNA segments than on longer ones (Brutzer et al., 2010). Furthermore, DNA bending stress has been shown to lower the elongation speed and processivity of the T7 phage RNAP (Lionberger and Meyhöfer, 2010).

The apparent switch from collaborative to antagonistic group behavior following promoter repression is accompanied by a significant increase in premature transcription termination (Figures 5C and 5D), presumably as a result of torsional stress (Figure S6E) and RNAP stalling (Fisher and Yanofsky, 1983;

Guarente and Beckwith, 1978; Jin et al., 1992; Kotlajich et al., 2015; McDowell et al., 1994; Peters et al., 2011; Yanofsky and Horn, 1981). Prior to our work, the general assumption was that promoter repression in response to a change in intracellular or environmental conditions stops the loading of RNAPs but does not affect the already-loaded RNAPs. These RNAPs were assumed to continue transcription elongation normally, creating a wasteful delay between promoter inactivation and protein synthesis arrest. This would be analogous to stopping a car by taking the foot off the accelerator and not using the brake. However, our study shows that transcription from a group of RNAPs provides a built-in brake that more rapidly halts the production of proteins that are no longer useful.

Our proposed mechanism also has implications for neighboring genes. It is already established that negative DNA supercoiling can promote the local unwinding of DNA and facilitate transcription initiation of a neighboring gene transcribed in the opposite direction (Dunaway and Ostrander, 1993; Meyer and Beslon, 2014; Naughton et al., 2013b; Opel and Hatfield, 2001; Rhee et al., 1999). We found that transcription-induced DNA supercoiling can have a negative effect on divergently expressed gene pairs, this time on transcription elongation (Figure 6). If a gene is strongly expressed, negative DNA supercoils created by RNAP translocation near the promoter can spread and impede the translocation of RNAPs on the neighboring, divergently transcribed gene (Figure 7B). This antagonistic effect can occur even when genes are separated by over 2 kb (Figure 6). Given the prevalence of divergent transcription in genomes (Wei et al., 2011), our result suggests another potential DNA supercoiling-dependent constraint on chromosomal gene arrangement during evolution (Meyer et al., 2018; Sobetzko, 2016). Our result also has implications for genetic engineering. Specifically, if fast transcription elongation is a desired property, one should avoid placing a pair of two strongly expressed genes in opposing orientations.

Given the implications of transcription-induced DNA supercoiling, it will be important to incorporate DNA torsional constraints into future mathematical models of transcription by multiple RNAPs. Although, to our knowledge, no previous theoretical works have shown or predicted our observations, recent studies have made steps forward by introducing DNA supercoiling effects into their models (Heberling et al., 2016; Sevier and Levine, 2018; Tantale et al., 2016). Expanding on these models will be important, especially if they are combined with experiments that quantitatively determine (1) how DNA torsional stress between two RNAPs changes as a function of the speed of these RNAPs and their in-between distance and (2) how DNA torsional stress affects the speed of these two RNAPs.

In conclusion, our work suggests that RNAP group dynamics emerge from transcription-induced DNA supercoiling, without evoking RNAP collision or convoy formation. We provide evidence that RNAPs affect each other over long (kb) distances, assisting or hindering each other's translocation depending on the status of the promoter (active or repressed) and therefore the needs of the cell. Long-distance RNAP dynamics can be both intragenic (Figures 1, 2, 3, 4, and 5) and intergenic (Figure 6). Our findings may be broadly applicable, given that transcription-induced DNA supercoiling is a common feature of living cells across domains of life (Giaever and Wang, 1988; Kouzine et al., 2014; Liu and Wang, 1987; Naughton et al., 2013a).

STAR★METHODS

Detailed methods are provided in the online version of this paper and include the following:

- KEY RESOURCES TABLE
- LEAD CONTACT AND MATERIALS AVAILABILITY
- EXPERIMENTAL MODEL AND SUBJECT DETAILS
  - Bacterial strains and growth conditions
- METHOD DETAILS
  - Induction and repression of *lacZ* expression
  - Miller assay
  - Two-color fluorescence *in situ* hybridization (FISH) microscopy
  - RNA extraction and real-time quantitative polymerase chain reaction (qPCR)
  - *In vitro* transcription
- QUANTIFICATION AND STATISTICAL ANALYSIS
  - Estimation of r_{ON} and r_{OFF}
  - (i) No-pause-site model
  - (ii) Pause-site model
  - FISH data analysis
  - mRNA fold change from qPCR
  - NET-seq data analysis
  - Statistical test
- DATA AND CODE AVAILABILITY

SUPPLEMENTAL INFORMATION

Supplemental Information can be found online at https://doi.org/10.1016/j.cell.2019.08.033.

ACKNOWLEDGMENTS

We thank Drs. Carol Gross, Jonathan Weissman, Matthew Larson, Hendrik Osadnik, and Jeff Hussmann for helpful discussions and technical help; Drs. Samuel Kou and Andrei Kuzminov for useful suggestions; Drs. Wayne Wade and Jeorg Bewersdorf for materials; and Dr. Andrew Goodman for allowing us to use his real-time PCR machine. We also thank Dr. Patricia Rosa and the members of the Jacobs-Wagner laboratory for discussions and critical reading of the manuscript. C.J.-W. is an Investigator of the Howard Hughes Medical Institute.

AUTHOR CONTRIBUTIONS

S.K. and C.J.-W. designed the study. S.K. performed experiments, and S.K., B.B., and C.J.-W. analyzed and discussed the data. S.K., B.B., and. I.I. provided resources. S.K. and C.J.-W. wrote the manuscript. All authors contributed to its editing.

DECLARATION OF INTERESTS

The authors declare no competing interests.

Received: September 19, 2018
Revised: June 14, 2019
Accepted: August 16, 2019
Published: September 19, 2019

SUPPORTING CITATIONS

The following references appear in the Supplemental Information: Datsenko and Wanner (2000); Gibson et al. (2009); Hui et al. (2015); Irnov and Winkler (2010); Sawitzke et al. (2013).

REFERENCES

Adesnik, M., and Levinthal, C. (1970). The synthesis and degradation of lactose operon messenger RNA in *E. coli*. Cold Spring Harb. Symp. Quant. Biol. *35*, 451–459.

Bachmann, B.J. (1972). Pedigrees of some mutant strains of Escherichia coli K-12. Bacteriol. Rev. *36*, 525–557.

Bai, L., Santangelo, T.J., and Wang, M.D. (2006). Single-molecule analysis of RNA polymerase transcription. Annu. Rev. Biophys. Biomol. Struct. *35*, 343–360.

Bon, M., McGowan, S.J., and Cook, P.R. (2006). Many expressed genes in bacteria and yeast are transcribed only once per cell cycle. FASEB J. *20*, 1721–1723.

Booker, B.M., Deng, S., and Higgins, N.P. (2010). DNA topology of highly transcribed operons in Salmonella enterica serovar Typhimurium. Mol. Microbiol. *78*, 1348–1364.

Bookout, A.L., Cummins, C.L., Mangelsdorf, D.J., Pesola, J.M., and Kramer, M.F. (2006). High-throughput real-time quantitative reverse transcription PCR. Curr. Protoc. Mol. Biol. *Chapter 15*, Unit 15.8.

Brutzer, H., Luzzietti, N., Klaue, D., and Seidel, R. (2010). Energetics at the DNA supercoiling transition. Biophys. J. *98*, 1267–1276.

Campbell, E.A., Korzheva, N., Mustaev, A., Murakami, K., Nair, S., Goldfarb, A., and Darst, S.A. (2001). Structural mechanism for rifampicin inhibition of bacterial rna polymerase. Cell *104*, 901–912.

Chong, S., Chen, C., Ge, H., and Xie, X.S. (2014). Mechanism of transcriptional bursting in bacteria. Cell *158*, 314–326.

Condon, C., French, S., Squires, C., and Squires, C.L. (1993). Depletion of functional ribosomal RNA operons in Escherichia coli causes increased expression of the remaining intact copies. EMBO J. *12*, 4305–4315.

Crut, A., Koster, D.A., Seidel, R., Wiggins, C.H., and Dekker, N.H. (2007). Fast dynamics of supercoiled DNA revealed by single-molecule experiments. Proc. Natl. Acad. Sci. USA *104*, 11957–11962.

Datsenko, K.A., and Wanner, B.L. (2000). One-step inactivation of chromosomal genes in Escherichia coli K-12 using PCR products. Proc. Natl. Acad. Sci. USA *97*, 6640–6645.

Deuschle, U., Kammerer, W., Gentz, R., and Bujard, H. (1986). Promoters of Escherichia coli: a hierarchy of in vivo strength indicates alternate structures. EMBO J. *5*, 2987–2994.

Dunaway, M., and Ostrander, E.A. (1993). Local domains of supercoiling activate a eukaryotic promoter in vivo. Nature *361*, 746–748.

Dykxhoorn, D.M., St Pierre, R., and Linn, T. (1996). A set of compatible tac promoter expression vectors. Gene *177*, 133–136.

Epshtein, V., and Nudler, E. (2003). Cooperation between RNA polymerase molecules in transcription elongation. Science *300*, 801–805.

Epshtein, V., Toulmé, F., Rahmouni, A.R., Borukhov, S., and Nudler, E. (2003). Transcription through the roadblocks: the role of RNA polymerase cooperation. EMBO J. *22*, 4719–4727.

Fisher, R.F., and Yanofsky, C. (1983). Mutations of the beta subunit of RNA polymerase alter both transcription pausing and transcription termination in the trp operon leader region in vitro. J. Biol. Chem. *258*, 8146–8150.

Forte, G., Caraglio, M., Marenduzzo, D., and Orlandini, E. (2019). Plectoneme dynamics and statistics in braided polymers. Phys. Rev. E *99*, 052503.

Ganji, M., Kim, S.H., van der Torre, J., Abbondanzieri, E., and Dekker, C. (2016). Intercalation-based single-molecule fluorescence assay to study DNA supercoil dynamics. Nano Lett. *16*, 4699–4707.

Giaever, G.N., and Wang, J.C. (1988). Supercoiling of intracellular DNA can occur in eukaryotic cells. Cell *55*, 849–856.

Gibson, D.G., Young, L., Chuang, R.-Y., Venter, J.C., Hutchison, C.A., 3rd, and Smith, H.O. (2009). Enzymatic assembly of DNA molecules up to several hundred kilobases. Nat. Methods *6*, 343–345.

Griffith, K.L., and Wolf, R.E., Jr. (2002). Measuring β-galactosidase activity in bacteria: cell growth, permeabilization, and enzyme assays in 96-well arrays. Biochem. Biophys. Res. Commun. *290*, 397–402.

Guarente, L.P., and Beckwith, J. (1978). Mutant RNA polymerase of Escherichia coli terminates transcription in strains making defective rho factor. Proc. Natl. Acad. Sci. USA *75*, 294–297.

Guptasarma, P. (1996). Cooperative relaxation of supercoils and periodic transcriptional initiation within polymerase batteries. BioEssays *18*, 325–332.

Heberling, T., Davis, L., Gedeon, J., Morgan, C., and Gedeon, T. (2016). A mechanistic model for cooperative behavior of co-transcribing RNA polymerases. PLoS Comput. Biol. *12*, e1005069.

Hui, S., Silverman, J.M., Chen, S.S., Erickson, D.W., Basan, M., Wang, J., Hwa, T., and Williamson, J.R. (2015). Quantitative proteomic analysis reveals a simple strategy of global resource allocation in bacteria. Mol. Syst. Biol. *11*, 784.

Irnov, I., and Winkler, W.C. (2010). A regulatory RNA required for antitermination of biofilm and capsular polysaccharide operons in Bacillales. Mol. Microbiol. *76*, 559–575.

Ivenso, I.D., and Lillian, T.D. (2016). Simulation of DNA supercoil relaxation. Biophys. J. *110*, 2176–2184.

Iyer, S., Park, B.R., and Kim, M. (2016). Absolute quantitative measurement of transcriptional kinetic parameters in vivo. Nucleic Acids Res. *44*, e142.

Jin, D.J., Burgess, R.R., Richardson, J.P., and Gross, C.A. (1992). Termination efficiency at rho-dependent terminators depends on kinetic coupling between RNA polymerase and rho. Proc. Natl. Acad. Sci. USA *89*, 1453–1457.

Jin, J., Bai, L., Johnson, D.S., Fulbright, R.M., Kireeva, M.L., Kashlev, M., and Wang, M.D. (2010). Synergistic action of RNA polymerases in overcoming the nucleosomal barrier. Nat. Struct. Mol. Biol. *17*, 745–752.

Jones, D.L., Brewster, R.C., and Phillips, R. (2014). Promoter architecture dictates cell-to-cell variability in gene expression. Science *346*, 1533–1536.

Joo, C., and Ha, T. (2012). Labeling DNA (or RNA) for single-molecule FRET. Cold Spring Harb. Protoc. *2012*, 1005–1008.

Kepes, A. (1969). Transcription and translation in the lactose operon of Escherichia coli studied by in vivo kinetics. Prog. Biophys. Mol. Biol. *19*, 199–236.

Kim, S., and Jacobs-Wagner, C. (2018). Effects of mRNA degradation and site-specific transcriptional pausing on protein expression noise. Biophys. J. *114*, 1718–1729.

Kohler, R., Mooney, R.A., Mills, D.J., Landick, R., and Cramer, P. (2017). Architecture of a transcribing-translating expressome. Science *356*, 194–197.

Koster, D.A., Crut, A., Shuman, S., Bjornsti, M.-A., and Dekker, N.H. (2010). Cellular strategies for regulating DNA supercoiling: a single-molecule perspective. Cell *142*, 519–530.

Kotlajich, M.V., Hron, D.R., Boudreau, B.A., Sun, Z., Lyubchenko, Y.L., and Landick, R. (2015). Bridged filaments of histone-like nucleoid structuring protein pause RNA polymerase and aid termination in bacteria. eLife *4*, e04970.

Kouzine, F., Gupta, A., Baranello, L., Wojtowicz, D., Ben-Aissa, K., Liu, J., Przytycka, T.M., and Levens, D. (2013). Transcription-dependent dynamic supercoiling is a short-range genomic force. Nat. Struct. Mol. Biol. *20*, 396–403.

Kouzine, F., Levens, D., and Baranello, L. (2014). DNA topology and transcription. Nucleus *5*, 195–202.

Kulaeva, O.I., Hsieh, F.-K., and Studitsky, V.M. (2010). RNA polymerase complexes cooperate to relieve the nucleosomal barrier and evict histones. Proc. Natl. Acad. Sci. USA *107*, 11325–11330.

Landick, R., Carey, J., and Yanofsky, C. (1985). Translation activates the paused transcription complex and restores transcription of the trp operon leader region. Proc. Natl. Acad. Sci. USA *82*, 4663–4667.

Larson, M.H., Landick, R., and Block, S.M. (2011). Single-molecule studies of RNA polymerase: one singular sensation, every little step it takes. Mol. Cell *41*, 249–262.

Larson, M.H., Mooney, R.A., Peters, J.M., Windgassen, T., Nayak, D., Gross, C.A., Block, S.M., Greenleaf, W.J., Landick, R., and Weissman, J.S. (2014). A pause sequence enriched at translation start sites drives transcription dynamics in vivo. Science *344*, 1042–1047.

Le, T.T., and Wang, M.D. (2018). Molecular highways—navigating collisions of DNA motor proteins. J. Mol. Biol. *430*, 4513–4524.

Leng, F., Chen, B., and Dunlap, D.D. (2011). Dividing a supercoiled DNA molecule into two independent topological domains. Proc. Natl. Acad. Sci. USA *108*, 19973–19978.

Lionberger, T.A., and Meyhöfer, E. (2010). Bending the rules of transcriptional repression: tightly looped DNA directly represses T7 RNA polymerase. Biophys. J. *99*, 1139–1148.

Liu, W., and Saint, D.A. (2002). A new quantitative method of real time reverse transcription polymerase chain reaction assay based on simulation of polymerase chain reaction kinetics. Anal. Biochem. *302*, 52–59.

Liu, L.F., and Wang, J.C. (1987). Supercoiling of the DNA template during transcription. Proc. Natl. Acad. Sci. USA *84*, 7024–7027.

Ma, J., Bai, L., and Wang, M.D. (2013). Transcription under torsion. Science *340*, 1580–1583.

Mason, P.B., and Struhl, K. (2005). Distinction and relationship between elongation rate and processivity of RNA polymerase II in vivo. Mol. Cell *17*, 831–840.

Mayer, A., di Iulio, J., Maleri, S., Eser, U., Vierstra, J., Reynolds, A., Sandstrom, R., Stamatoyannopoulos, J.A., and Churchman, L.S. (2015). Native elongating transcript sequencing reveals human transcriptional activity at nucleotide resolution. Cell *161*, 541–554.

McClure, W.R., and Cech, C.L. (1978). On the mechanism of rifampicin inhibition of RNA synthesis. J. Biol. Chem. *253*, 8949–8956.

McDowell, J.C., Roberts, J.W., Jin, D.J., and Gross, C. (1994). Determination of intrinsic transcription termination efficiency by RNA polymerase elongation rate. Science *266*, 822–825.

Meyer, S., and Beslon, G. (2014). Torsion-mediated interaction between adjacent genes. PLoS Comput. Biol. *10*, e1003785.

Meyer, S., Reverchon, S., Nasser, W., and Muskhelishvili, G. (2018). Chromosomal organization of transcription: in a nutshell. Curr. Genet. *64*, 555–565.

Miller, J.H. (1972). Assay of β-galactosidase. In Experiments in Molecular Genetics (Cold Spring Harbor Laboratory), pp. 352–355.

Miller, O.L., Jr., Hamkalo, B.A., and Thomas, C.A., Jr. (1970). Visualization of bacterial genes in action. Science *169*, 392–395.

Min, I.M., Waterfall, J.J., Core, L.J., Munroe, R.J., Schimenti, J., and Lis, J.T. (2011). Regulating RNA polymerase pausing and transcription elongation in embryonic stem cells. Genes Dev. *25*, 742–754.

Mokry, M., Hatzis, P., Schuijers, J., Lansu, N., Ruzius, F.-P., Clevers, H., and Cuppen, E. (2012). Integrated genome-wide analysis of transcription factor occupancy, RNA polymerase II binding and steady-state RNA levels identify differentially regulated functional gene classes. Nucleic Acids Res. *40*, 148–158.

Monod, J. (1956). Remarks on the mechanism of enzyme induction. In Enzymes: Units of Biological Structure and Function, O.H. Gaebler, ed. (Academic Press), pp. 7–28.

Montero Llopis, P., Jackson, A.F., Sliusarenko, O., Surovtsev, I., Heinritz, J., Emonet, T., and Jacobs-Wagner, C. (2010). Spatial organization of the flow of genetic information in bacteria. Nature *466*, 77–81.

Mooney, R.A., Davis, S.E., Peters, J.M., Rowland, J.L., Ansari, A.Z., and Landick, R. (2009). Regulator trafficking on bacterial transcription units in vivo. Mol. Cell *33*, 97–108.

Mosteller, R.D., and Yanofsky, C. (1970). Transcription of the tryptophan operon in Escherichia coli: rifampicin as an inhibitor of initiation. J. Mol. Biol. *48*, 525–531.

Naughton, C., Avlonitis, N., Corless, S., Prendergast, J.G., Mati, I.K., Eijk, P.P., Cockroft, S.L., Bradley, M., Ylstra, B., and Gilbert, N. (2013a). Transcription forms and remodels supercoiling domains unfolding large-scale chromatin structures. Nat. Struct. Mol. Biol. *20*, 387–395.

Naughton, C., Corless, S., and Gilbert, N. (2013b). Divergent RNA transcription: a role in promoter unwinding? Transcription *4*, 162–166.

Nelson, P. (1999). Transport of torsional stress in DNA. Proc. Natl. Acad. Sci. USA *96*, 14342–14347.

Noel, R.J., Jr., and Reznikoff, W.S. (2000). Structural studies of lacUV5-RNA polymerase interactions in vitro. Ethylation interference and missing nucleoside analysis. J. Biol. Chem. *275*, 7708–7712.

Novick, A., and Weiner, M. (1957). Enzyme induction as an all-or-none phenomenon. Proc. Natl. Acad. Sci. USA *43*, 553–566.

Opel, M.L., and Hatfield, G.W. (2001). DNA supercoiling-dependent transcriptional coupling between the divergently transcribed promoters of the ilvYC operon of Escherichia coli is proportional to promoter strengths and transcript lengths. Mol. Microbiol. *39*, 191–198.

Ozbudak, E.M., Thattai, M., Lim, H.N., Shraiman, B.I., and Van Oudenaarden, A. (2004). Multistability in the lactose utilization network of Escherichia coli. Nature *427*, 737–740.

Pelechano, V., Jimeno-González, S., Rodríguez-Gil, A., García-Martínez, J., Pérez-Ortín, J.E., and Chávez, S. (2009). Regulon-specific control of transcription elongation across the yeast genome. PLoS Genet. *5*, e1000614.

Pelechano, V., Chávez, S., and Pérez-Ortín, J.E. (2010). A complete set of nascent transcription rates for yeast genes. PLoS ONE *5*, e15442.

Peters, J.M., Vangeloff, A.D., and Landick, R. (2011). Bacterial transcription terminators: the RNA 3′-end chronicles. J. Mol. Biol. *412*, 793–813.

Proshkin, S., Rahmouni, A.R., Mironov, A., and Nudler, E. (2010). Cooperation between translating ribosomes and RNA polymerase in transcription elongation. Science *328*, 504–508.

Rhee, K.Y., Opel, M., Ito, E., Hung, Sp., Arfin, S.M., and Hatfield, G.W. (1999). Transcriptional coupling between the divergent promoters of a prototypic LysR-type regulatory system, the ilvYC operon of Escherichia coli. Proc. Natl. Acad. Sci. USA *96*, 14294–14299.

Rovinskiy, N., Agbleke, A.A., Chesnokova, O., Pang, Z., and Higgins, N.P. (2012). Rates of gyrase supercoiling and transcription elongation control supercoil density in a bacterial chromosome. PLoS Genet. *8*, e1002845.

Ryals, J., Little, R., and Bremer, H. (1982). Temperature dependence of RNA synthesis parameters in Escherichia coli. J. Bacteriol. *151*, 879–887.

Saeki, H., and Svejstrup, J.Q. (2009). Stability, flexibility, and dynamic interactions of colliding RNA polymerase II elongation complexes. Mol. Cell *35*, 191–205.

Sawitzke, J.A., Thomason, L.C., Bubunenko, M., Li, X., Costantino, N., and Court, D.L. (2013). Chapter seven - Recombineering: using drug cassettes to knock out genes in vivo. In Methods in Enzymology, J. Lorsch, ed. (Academic Press), pp. 79–102.

Schleif, R., Hess, W., Finkelstein, S., and Ellis, D. (1973). Induction kinetics of the L-arabinose operon of Escherichia coli. J. Bacteriol. *115*, 9–14.

Schwanhäusser, B., Busse, D., Li, N., Dittmar, G., Schuchhardt, J., Wolf, J., Chen, W., and Selbach, M. (2011). Global quantification of mammalian gene expression control. Nature *473*, 337–342.

Sevier, S.A., and Levine, H. (2018). Properties of gene expression and chromatin structure with mechanically regulated elongation. Nucleic Acids Res. *46*, 5924–5934.

Sliusarenko, O., Heinritz, J., Emonet, T., and Jacobs-Wagner, C. (2011). High-throughput, subpixel precision analysis of bacterial morphogenesis and intracellular spatio-temporal dynamics. Mol. Microbiol. *80*, 612–627.

So, L.H., Ghosh, A., Zong, C., Sepúlveda, L.A., Segev, R., and Golding, I. (2011). General properties of transcriptional time series in Escherichia coli. Nat. Genet. *43*, 554–560.

Sobetzko, P. (2016). Transcription-coupled DNA supercoiling dictates the chromosomal arrangement of bacterial genes. Nucleic Acids Res. *44*, 1514–1524.

Taniguchi, Y., Choi, P.J., Li, G.W., Chen, H., Babu, M., Hearn, J., Emili, A., and Xie, X.S. (2010). Quantifying E. coli proteome and transcriptome with single-molecule sensitivity in single cells. Science *329*, 533–538.

Tantale, K., Mueller, F., Kozulic-Pirher, A., Lesne, A., Victor, J.-M., Robert, M.-C., Capozi, S., Chouaib, R., Bäcker, V., Mateos-Langerak, J., et al. (2016). A single-molecule view of transcription reveals convoys of RNA polymerases and multi-scale bursting. Nat. Commun. *7*, 12248.

Tsao, Y.-P., Wu, H.-Y., and Liu, L.F. (1989). Transcription-driven supercoiling of DNA: direct biochemical evidence from in vitro studies. Cell *56*, 111–118.

van Loenhout, M.T.J., de Grunt, M.V., and Dekker, C. (2012). Dynamics of DNA supercoils. Science *338*, 94–97.

Vijayan, V., Jain, I.H., and O'Shea, E.K. (2011). A high resolution map of a cyanobacterial transcriptome. Genome Biol. *12*, R47.

Vogel, U., and Jensen, K.F. (1994). Effects of guanosine 3′,5′-bisdiphosphate (ppGpp) on rate of transcription elongation in isoleucine-starved Escherichia coli. J. Biol. Chem. *269*, 16236–16241.

Vogel, U., and Jensen, K.F. (1997). NusA is required for ribosomal antitermination and for modulation of the transcription elongation rate of both antiterminated RNA and mRNA. J. Biol. Chem. *272*, 12265–12271.

Voulgaris, J., French, S., Gourse, R.L., Squires, C., and Squires, C.L. (1999). Increased rrn gene dosage causes intermittent transcription of rRNA in Escherichia coli. J. Bacteriol. *181*, 4170–4175.

Wade, J.T., and Struhl, K. (2004). Association of RNA polymerase with transcribed regions in Escherichia coli. Proc. Natl. Acad. Sci. USA *101*, 17777–17782.

Wang, Z., and Dröge, P. (1997). Long-range effects in a supercoiled DNA domain generated by transcription in vitro. J. Mol. Biol. *271*, 499–510.

Wei, W., Pelechano, V., Järvelin, A.I., and Steinmetz, L.M. (2011). Functional consequences of bidirectional promoters. Trends Genet. *27*, 267–276.

Yanofsky, C., and Horn, V. (1981). Rifampin resistance mutations that alter the efficiency of transcription termination at the tryptophan operon attenuator. J. Bacteriol. *145*, 1334–1341.

STAR★METHODS

KEY RESOURCES TABLE

REAGENT or RESOURCE	SOURCE	IDENTIFIER
Bacterial Strains		
Escherichia coli MG1655	Bachmann, 1972	(Wild-type)
MG1655 Δ*lacYA*	This paper	CJW5461
MG1655 Δ*lacIZYA*/pEXT22-lacI-lacZYA	This paper	CJW5616
MG1655 Δ*lacIZYA*	This paper	CJW6643
MG1655 Δ*lacIZYA*/pUC19-lacI-lacZ	This paper	CJW6647
DH5α/pUC19-lacI-P_{lacUV5}-lacZYA	This paper	CJW6770
MG1655 pUC19-P_{tet}-gfp	This paper	CJW6919
MG1655 pUC19-P_{tet}-topA	This paper	CJW6920
MG1655 pUC19-P_{tet}-trpC	This paper	CJW6986
MG1655 Δ*lacIZYA*/pUC19-lacI(O3-)-L220-$P_{ompA,M1}$-mgfp (reverse)-lacZ	This paper	CJW6988
MG1655 Δ*lacIZYA*/pUC19-lacI(O3-)-L400-$P_{ompA,M1}$-mgfp (reverse)-lacZ	This paper	CJW6987
MG1655 Δ*lacIZYA*/pUC19-lacI(O3-)-L900-$P_{ompA,M1}$-mgfp (reverse)-lacZ	This paper	CJW6989
MG1655 Δ*lacIZYA*/pUC19-lacI(O3-)-L1400-$P_{ompA,M1}$-mgfp (reverse)-lacZ	This paper	CJW6990
MG1655 Δ*lacIZYA*/pUC19-lacI(O3-)-L1900-$P_{ompA,M1}$-mgfp (reverse)-lacZ	This paper	CJW6991
MG1655 Δ*lacIZYA*/pUC19-lacI(O3-)-L2400-$P_{ompA,M1}$-mgfp (reverse)-lacZ	This paper	CJW6992
MG1655 Δ*lacIZYA*/pUC19-lacI(O3-)-L220-$P_{ompA,M5}$-mgfp(reverse)-lacZ	This paper	CJW6999
MG1655 Δ*lacIZYA*/pUC19-lacI(O3-)-L400-$P_{ompA,M5}$-*mgfp*(reverse)-*lacZ*	This paper	CJW6998
MG1655 Δ*lacIZYA*/pUC19-lacI(O3-)-L900-$P_{ompA,M5}$-mgfp(reverse)-lacZ	This paper	CJW6993
MG1655 Δ*lacIZYA*/pUC19-lacI(O3-)-L1400-$P_{ompA,M5}$-mgfp(reverse)-lacZ	This paper	CJW6994
MG1655 Δ*lacIZYA*/pUC19-lacI(O3-)-L1900-$P_{ompA,M5}$-mgfp(reverse)-lacZ	This paper	CJW6995
MG1655 Δ*lacIZYA*/pUC19-lacI(O3-)-L2400-$P_{ompA,M5}$-mgfp(reverse)-lacZ	This paper	CJW6996
Chemicals, Peptides, and Recombinant Proteins		
Acid-phenol:chloroform (pH 4.5 with isoamyl alcohol, 125:24:1)	Invitrogen	Cat#AM9722
Anhydrotetracyclin, hydrochloride (aTc)	Cayman Chemical	Cat#10009542
ApA RNA dinucleotide	TriLink Biotechnologies	Cat#O-31001
Bovine serum albumin (BSA)	Sigma-Aldrich	Cat#B2518
Cy3B NHS ester	GE Healthcare Life Sciences	Cat#PA63101
Cy5 NHS ester	GE Healthcare Life Sciences	Cat#PA15101
Dextran sulfate	Millipore	Cat#S4030
E. coli RNA polymerase, holoenzyme	New England Biolabs	Cat#M0551S
E. coli topoisomerase I	New England Biolabs	Cat#M0301S
E. coli tRNA	Sigma-Aldrich	Cat#R1753
EcoRI-HF restriction endonuclease	New England Biolabs	Cat#R3101
Formaldehyde	Ladd Research Industries	Cat#20295
Formamide	American Bio	Cat#AB00600
Glycogen, Ultrapure™	Invitrogen	Cat#10814010
Isopropylthio-β-galactoside (IPTG)	Invitrogen	Cat#15529019
KAPA SYBR FAST one-step qRT-PCR kit	Kapa Biosystems	Cat#KK4652
LB broth, Miller	Fisher Bioreagents	Cat#BP1426-2
MOPS EZ rich defined medium	Teknova	Cat#M2105
2-Nitrophenyl β-D-fucopyranoside (ONPF)	Santa Cruz Biotechnology	Cat#sc-216258
Ortho-nitrophenyl-β-galactoside (ONPG)	Thermo Scientific	Cat#34055
NTP mix	Thermo Scientific	Cat#R0481

(*Continued on next page*)

Continued

REAGENT or RESOURCE	SOURCE	IDENTIFIER
Picodent twinsil 22	Picodent	Cat#1300 1000
Poly-L-lysine	Sigma-Aldrich	Cat#P8920
Protector RNase inhibitor	Roche	Cat#3335399001
Rifampicin (rif)	Sigma-Aldrich	Cat#R3501
RNA clean and concentrator-5	Zymo Research	Cat#R1016
Saline-sodium citrate buffer (SSC)	Invitrogen	Cat#AM9763
Super PAP Pen	Invitrogen	Cat#008899
Trizol	Invitrogen	Cat#15596018
Turbo DNase	Invitrogen	Cat#AM2238
Vanadyl ribonucleoside complex (VRC)	Sigma-Aldrich	Cat#94742
Deposited Data		
E. coli RNAP profiling data	Larson et al., 2014	GSE56720 GSM1367304
MATLAB code for analyzing smFISH images, Miller assay, and RNAP profiling data	This paper	https://www.github.com/JacobsWagnerLab/published
Oligonucleotides		
FISH probes	Biosearch Technologies	See Tables S2 and S3
Primers for qPCR	Integrated DNA Technologies	See Table S4
Recombinant DNA		
pEXT22-lacI-lacZYA	This paper	See Data S1
pUC19-lacI-lacZ	This paper	See Data S1
pUC19-lacI-P_{lacUV5}-lacZYA	This paper	See Data S1
pUC19-P_{tet}-gfp	This paper	See Data S1
pUC19-P_{tet}-topA	This paper	See Data S1
pUC19-P_{tet}-trpC	This paper	See Data S1
pUC19-lacI(O3-)-L220-$P_{ompA,M1}$-mgfp(reverse)-lacZ	This paper	See Data S1
pUC19-lacI(O3-)-L400-$P_{ompA,M1}$-mgfp(reverse)-lacZ	This paper	See Data S1
pUC19-lacI(O3-)-L900-$P_{ompA,M1}$-mgfp(reverse)-lacZ	This paper	See Data S1
pUC19-lacI(O3-)-L1400-$P_{ompA,M1}$-mgfp(reverse)-lacZ	This paper	See Data S1
pUC19-lacI(O3-)-L1900-$P_{ompA,M1}$-mgfp(reverse)-lacZ	This paper	See Data S1
pUC19-lacI(O3-)-L2400-$P_{ompA,M1}$-mgfp(reverse)-lacZ	This paper	See Data S1
pUC19-lacI(O3-)-L220-$P_{ompA,M5}$-mgfp(reverse)-lacZ	This paper	See Data S1
pUC19-lacI(O3-)-L400-$P_{ompA,M5}$-mgfp(reverse)-lacZ	This paper	See Data S1
pUC19-lacI(O3-)-L900-$P_{ompA,M5}$-mgfp(reverse)-lacZ	This paper	See Data S1
pUC19-lacI(O3-)-L1400-$P_{ompA,M5}$-mgfp(reverse)-lacZ	This paper	See Data S1
pUC19-lacI(O3-)-L1900-$P_{ompA,M5}$-mgfp(reverse)-lacZ	This paper	See Data S1
pUC19-lacI(O3-)-L2400-$P_{ompA,M5}$-mgfp(reverse)-lacZ	This paper	See Data S1
Software and Algorithms		
Igor Pro	WaveMetrics	https://www.wavemetrics.com
MATLAB	Mathworks	https://www.mathworks.com
MicrobeTracker	Sliusarenko et al., 2011	https://www.github.com/JacobsWagnerLab/MicrobeTracker and http://www.microbetracker.org/

LEAD CONTACT AND MATERIALS AVAILABILITY

The reagents generated in this study are available without restriction. Further information and requests for resources and reagents should be directed to and will be fulfilled by the Lead Contact, Christine Jacobs-Wagner (christine.jacobs-wagner@yale.edu).

EXPERIMENTAL MODEL AND SUBJECT DETAILS

Bacterial strains and growth conditions

A complete list of strains and plasmids used in this study is provided in Table S1 along with a brief description of their construction. Experiments were primarily performed on wild-type *Escherichia coli* MG1655 cells unless noted otherwise. All constructs made in this study were verified by sequencing the engineered DNA regions. Plasmid sequence files (Data S1) are provided in a Zip file as supplemental information.

In all experiments, with some noted exceptions (see below), *E. coli* cells were grown in liquid cultures (~20 mL) of M9 minimal medium (6 g/L dibasic sodium phosphate anhydrous, 3 g/L monobasic potassium phosphate, 0.5 g/L sodium chloride, 1 g/L ammonium chloride, 2 mM magnesium sulfate, 0.1 mM calcium chloride) supplemented with 0.2% glycerol, 0.1% casamino acids (Difco Laboratories) and 1 mg/L thiamine (M9glyCaaT) at 30°C using a water bath shaker. Appropriate antibiotics were added to cultures of strains carrying a plasmid (Table S1). Overnight stationary cultures were diluted > 1000 fold in the same growth medium (with antibiotics when appropriate) and experiments were performed (e.g., induction of *lacZ* expression) when the culture was in exponential growth phase (optical density at 600 nm, OD_{600}, was about 0.2).

In some instances, cells were grown in different media. MOPS EZ rich defined medium supplemented with 0.2% glucose was made according to the instruction of the manufacturer (Teknova). LB medium was made from commercial Miller's LB broth powder (Fisher Bioreagents).

METHOD DETAILS

Induction and repression of *lacZ* expression

For induction, IPTG (Invitrogen) was added to the *E. coli* culture to a final concentration of 0.02-1 mM as indicated in the text and figures. This event marks time zero (t = 0 s). Cell cultures, shaken in a water bath at 30°C, were sampled thereafter at the indicated time points. The shaking was interrupted only when chemicals were added to the cultures or when samples were taken. To turn off the *lac* promoter, we used three independent methods by adding either 5 mM ONPF (Santa Cruz Biotechnology) at t = 90 s, 500 mM glucose (Fisher Bioreagents) at t = 90 s, or 400 μg/mL rifampicin at t = 40 s. ONPF was used to turn off the promoter when 0.05 mM IPTG was added for Miller assay experiments, and glucose was used to turn off the promoter when 0.2 mM IPTG was added for Miller assay experiments, as well as in all FISH experiments for reasons indicated below. The fact that Z5 mRNA signal peaked at t = 2 min after glucose addition at t = 90 s (Figure 2D) indicates that the *lac* promoter was turned off almost immediately after glucose addition. We observed the same result in FISH experiments when 5 mM ONPF was added after induction with 0.05 mM IPTG (Figure S3C). When the promoter was turned off, LacZ activity leveled off after t ~6 min in the Miller assay, as expected (Figures S2B, S2D, and S5D).

Note that we found that 5 mM ONPF was not sufficient to turn off the *lac* promoter when it was induced with 0.2 mM IPTG, for which condition we then primarily used 500 mM glucose. When glucose was used to turn off the promoter, we washed the cells before performing the Miller assay because glucose affected the enzymatic reaction of LacZ with the colorimetric substrate. This step was not required for FISH experiments.

Miller assay

We followed a previously described procedure (Griffith and Wolf, 2002; Kim and Jacobs-Wagner, 2018; Miller, 1972). In short, 300 μL of culture were taken every 20-60 s after the addition of IPTG and transferred to a 1.5-mL tube containing 37 μL of chloramphenicol (5 mg/mL stock in 10% ethanol). The tubes were kept on ice throughout the remaining procedure (Griffith and Wolf, 2002). If glucose was added to turn off the *lac* promoter, cells were washed at this stage. For washing, the Eppendorf tubes were spun at 4,500 x g for 4 min at room temperature and cell pellets were resuspended in cold fresh medium supplemented with chloramphenicol (0.5 mg/mL).

To measure the relative amount of cells in each culture sample, 190 μL cell cultures from each tube were transferred to a 96-well plate and OD_{600} was measured at 30°C in a microplate reader (Synergy2, BioTek). OD_{600} was measured every 5 min for 25 min. Cells did not grow during this time period due to the chloramphenicol treatment. An average of five measurements was used as a normalization factor for cell density. Next, the remaining cells in the tubes were lysed by adding 50 μL of lysis buffer (60 mM disodium phosphate, 40 mM monosodium phosphate, 10 mM potassium chloride, 1 mM magnesium sulfate, 0.0075% sodium dodecyl sulfate, plus 188 mM β-mercaptoethanol) and 20 μL of chloroform. After lysis, 160 μL of the supernatant was transferred to a new 96-well plate. Lastly, 40 μL of ortho-nitrophenyl-β-galactoside (ONPG) solution (Thermo Scientific; 4 mg/mL stock in the lysis buffer) was added to each well. The color change caused by hydrolysis of ONPG by LacZ was monitored by measuring absorbance at 420 nm at 30°C in the microplate reader. Absorbance at 550 nm was measured at the same time to account for cell debris. LacZ activity was calculated as:

$$LacZ\ activity = 1000 \times \frac{OD_{420} - 1.75 \times OD_{550}}{t \times OD_{600}} \times dilution\ factor \quad (1)$$

Here, t is the ONPG reaction time in minutes and OD indicates optical density measurements. The dilution factor is the fraction of cell lysates in the final volume of the ONPG reaction. In our case, the fraction was 0.6.

For data analysis, we first determined a baseline by doing a least-squares fit of a line of zero slope from $t = 0$ s (time of IPTG addition) to the start of LacZ appearance ($y = c$). Then, the baseline LacZ activity was subtracted to show the change in LacZ activity from the basal level. Next, the square root of LacZ activity was plotted because LacZ amount is expected to increase as a function of t^2 (Schleif et al., 1973). We performed a least-squares fit of a line ($y = a + bx$; Igor Pro (WaveMetrics)) to the initial increase in square root of LacZ activity. The intercept of this line with the x axis, or $-a/b$, gives the time of LacZ appearance (e.g., Figure S1B).

Once a fitted line ($y = a + bx$) was determined for each independent time-course Miller assay experiment, the average and standard deviation of the fits were calculated and plotted to show LacZ expression kinetics upon induction (Figures 1B, 2A, 4A, 4G, and S3B).

Two-color fluorescence *in situ* hybridization (FISH) microscopy

We followed a procedure previously published (Kim and Jacobs-Wagner, 2018). Briefly, 750 μL of culture were taken every minute after the addition of IPTG and immediately transferred to a 1.5-mL tube containing 4x fixing solution made of 16% formaldehyde (Ladd Research Industries) in sodium phosphate buffer at pH 7.4. For the time-zero samples in particular, a cell sample was taken before IPTG addition. Cells were fixed for 15 min at room temperature and 30 min on ice. Next, the fixed cells were washed with diethyl pyrocarbonate (DEPC)-treated phosphate buffered saline (PBS) three times by performing centrifugation (4,500 x g) for 4 min at room temperature, after which cells were applied onto individual wells on coverslips coated with 0.1% poly-L-lysine. Individual wells were drawn by a water-repellent marker (Super PAP Pen, Invitrogen). All the remaining procedures were performed while the cells adhered to the coverslip.

Cells were permeabilized with 70% ethanol for 5 min. Before probe hybridization, cells were incubated with a prehybridization solution containing 20% formamide (American Bio), 2x saline-sodium citrate buffer (2x SSC; 300 mM sodium chloride, 30 mM sodium citrate, pH 7.0, Invitrogen), and 0.2 mM vanadyl ribonucleoside complex (VRC) for 30 min at 37°C.

The hybridization solution consisted of 4 nM of probes in 20% formamide, 2x SSC, 0.2 mM VRC, 10% dextran sulfate, 0.1% bovine serum albumin, and 0.4 mg/mL *E. coli* tRNA. The solution was applied to cells for 2 h at 37°C. After washing with wash solution (25% formamide and 2x SSC) and DEPC-PBS five times each, DEPC-PBS was applied onto the sample, and the coverslip was mounted on a glass slide. It was sealed with pliable silicone (picodent, a gift from Dr. Joerg Bewersdorf). Imaging by phase contrast and fluorescence microscopy was performed on an Eclipse Ti microscope (Nikon) equipped with a Sola LE light source (Lumencor), a phase-contrast objective Plan Apochromat 100 × /1.45 NA (Nikon) and an Orca-II-ER CCD camera (Hamamatsu Photonics). All images were acquired using the Nikon Elements software (Nikon).

The FISH probes were 20-nt-long oligonucleotides, 5′ end modified with amino-modifier C6 (Biosearch Technologies; see the list of sequences in Tables S2 and S3). Twenty-four probes complementary to the first and last 1-kb regions of *lacZ* were pooled together and named Z5 and Z3 probes, respectively. Z5 and Z3 probes were labeled with Cy5-NHS ester and Cy3B-NHS ester (GE Healthcare Life Sciences), respectively, following a previously described procedure (Joo and Ha, 2012). Fluorescently-labeled probes were then purified by ultra-performance liquid chromatography (Acquity UPLC system, Waters) on an Acquity BEH C18 column. The eluents were A: 100 mM triethylammonium acetate in milli-Q water and B: 100% acetonitrile. The gradient was set as follows: 0-5 min with 0% B, 5-35 min with a 0%–30% linear gradient of B, 35-37 min with a 30%–100% linear gradient of B, and 37-40 min with 0% B. The flow rate was kept at 0.1 mL/min. Chromatograms were recorded at 260 and 646 nm (for Cy5 labeling) or at 260 and 550 nm (for Cy3B labeling). The purified probes were lyophilized and resuspended in TE buffer (10 mM Tris-HCl pH 7.5 with 1 mM EDTA) to yield 4-5 μM stock solutions.

RNA extraction and real-time quantitative polymerase chain reaction (qPCR)

To examine the rate of transcription elongation of *trpC* and *gfp*, we performed time-course experiments in which expression of *trpC* (strain CJW6986) and *gfp* (strain CJW6919) from the anhytetracycline (aTC)-inducible promoter was induced with 100 ng/mL aTc at time zero. To have enough time delay between 5′ end and 3′ end mRNA appearance, both strains were grown at 25°C. CJW6986 was grown in LB to suppress expression of endogenous *trpC* whereas CJW6919 was grown in M9glyCaaT.

The mRNA levels of *trpC* and *gfp* were measured every 30 s for 4-5 min. When appropriate, rifampicin was added to the culture at a final concentration of 400 μg/mL to stop transcription initiation.

At each time point, 0.75 mL *E. coli* cell cultures (growth conditions are specified in Figure 2F) were taken and mixed with an equal volume of Trizol (Invitrogen) and vigorously shaken. The mixture was incubated for 5 min at room temperature, followed by 3-min incubation at 65°C and 15-min centrifugation at 20,000 x g at 4°C. The top aqueous phase (1 mL) was mixed with 0.8 mL isopropanol as well as 1 μL glycogen (Invitrogen) in a clean Eppendorf tube. Then, the mixture was incubated for 10 min at room temperature and centrifuged for 10 min at 20,000 x g at 4°C. The pellet was washed with cold 70% EtOH twice and air-dried. The pellet was dissolved in 50 μL of 1X Turbo DNase buffer (Thermo Fisher Scientific). One unit of Turbo DNase (Thermo Fisher Scientific) was added and incubated at 37°C for 60 min to remove any DNA. RNA was then purified using the RNA clean and concentrator-5 kit (Zymo Research) and the eluent was used for qPCR reactions (Kapa Biosystems) following the manufacturer's protocol. Primer sequences for 5′ end and 3′ end mRNA regions are provided in Table S4. The cycling parameters used were: 42°C for 5 min, 95°C for 3 min, 40 cycles of 95°C for 3 s and 60°C for 20 s, using a BioRad CFX96 Real-Time PCR instrument.

In vitro transcription

In vitro transcription reactions included the following: 0.24 pmol of plasmid DNA (prepared from strain CJW6770) in a 300 μL solution of *E. coli* RNA polymerase reaction buffer from New England Biolabs (40 mM Tris, 150 mM potassium chloride, 10 mM magnesium chloride, 1 mM dithiothreitol, 0.01% Triton X-100, pH 7.5 at 25°C), 90 μg/mL bovine serum albumin and 1 mM NTP mix (Thermo Scientific), supplemented with 75 units of RNase inhibitor (Roche). The Eppendorf tube containing this solution was incubated in a bench-top shaker at 37°C for 20 min before the next procedure.

At time zero, ~60 pmol of *E. coli* RNAP holoenzyme (New England Biolabs) was added and immediately mixed by pipetting. Eppendorf tubes were kept in the shaker at 37°C while aliquots of 35 μL were taken every 30 s. When appropriate, rifampicin was added at a final concentration of 400 μg/mL at t = 30 s to stop transcription initiation.

The aliquots were immediately pipetted into individual tubes containing acid-phenol:chloroform (pH 4.5 with isoamyl alcohol, 125:24:1, Invitrogen) to stop the reaction. After phenol:chloroform extraction, the samples underwent ethanol precipitation and pellets were dissolved in 50 μL of 1X Turbo DNase buffer (Invitrogen). The remaining procedure includes Turbo DNase reaction, RNA purification and qPCR as described in the previous section.

To examine the effect of negative DNA supercoiling on the rate of transcription elongation, 24 pmol of purified *E. coli* topoisomerase I (New England Biolabs) was added to the reaction mixture right before RNAP addition.

For *in vitro* transcription on a linear template, we used 0.24 pmol of linearized plasmid, prepared by cutting the plasmid extracted from CJW6770 cells with the restriction enzyme EcoRI. The reaction mixture also included ApA RNA dinucleotide (TriLink Biotechnologies) at a high concentration (1 mM) to allow multiple rounds of RNAP loading.

QUANTIFICATION AND STATISTICAL ANALYSIS

Estimation of r_{ON} and r_{OFF}

We calculated the rate of transcription elongation on the same region of *lacZ* depending on the promoter's ON or OFF status (r_{ON} versus r_{OFF}). Specifically, r_{OFF} is the speed of the first RNAPs from t = 90 s (when the anti-inducer was added) to the end of transcription in promoter-repression experiments. Assuming no pause sites, r_{ON} represents the overall speed of RNAPs when the promoter remains active, as shown schematically in Figure 2B.

We calculated r_{ON} and r_{OFF} from Miller assay and FISH experiments using a model that assumes either the absence of RNAP pause sites (no-pause-site model) or the presence of pause sites along the *lacZ* DNA template (pause-site model).

(i) No-pause-site model

Miller assays measure the total time that the first loaded RNAPs take to complete *lacZ* transcription (T_{ON} when the promoter remains active and $T_{ON\rightarrow OFF}$ when the promoter is repressed at t = 90 s). When the promoter is continuously active, the overall transcription elongation rate of the 3072-bp *lacZ* gene is calculated as follows.

$$r_{ON} = 3072/T_{ON} \tag{2}$$

Assuming there is no pause site, RNAPs translocate at this constant speed r_{ON} along the gene while the promoter remains active (Figure 2B). In the promoter-repression experiment, RNAPs translocate at r_{ON} from t = 0 to 90 s. From t = 90 s to the end of *lacZ* transcription (i.e., $t = T_{ON\rightarrow OFF}$), their apparent speed is reduced to r_{OFF}, explaining $T_{ON\rightarrow OFF}$ being larger than T_{ON} (Figure 2B). We calculated r_{OFF}, the average rate of transcription elongation after promoter repression, as:

$$r_{OFF} = \frac{3072 - 90 \cdot r_{ON}}{T_{ON\rightarrow OFF} - 90} \tag{3}$$

Here, r_{ON} and $T_{ON\rightarrow OFF}$ represent the mean of three or more measurements. The standard deviations associated with r_{ON} and $T_{ON\rightarrow OFF}$ were propagated to obtain the uncertainty of r_{OFF}.

FISH experiments measure the time delay of appearance between the Z5 and Z3 mRNA signals. We calculate r_{ON} as 2000 nt (distance between the mid-points of the Z3 and Z5 regions) divided by the time delay measured in the experiment when the promoter remains active. $T_{ON\rightarrow OFF}$ is calculated as the time delay measured in a promoter-repression experiment, multiplied by 3072/2000. Finally, Equation 3 is applied to obtain r_{OFF} in the same manner as for the Miller assays.

(ii) Pause-site model

We used the published nascent 3′ RNA sequencing (NET-seq) data (GSE56720) (Larson et al., 2014) to get relative dwell time of RNAPs at each base position along *lacZ* (Figure S2E). We removed read bias at x = 194 nt (x = 1 is the first base of the 3072 nt-long coding region) because the total RNA sequencing performed in the same study showed high reads at the position. For this and other base positions without reads (28 out of 3072), we used an interpolation function in MATLAB (interp1) to have reads in every base position.

Figure S2F shows a trajectory of RNAPs assuming "no pause" versus "with pause" according to the NET-seq measurements. Given that the first RNAPs take T_{ON} to transcribe 3072 bp of DNA, their position at t = 90 s (x_{90}) can be different depending on the assumption. It is closer to the promoter in the pause-site model (Figure S2F).

We defined r_{ON} as RNAP speed from t = 90 s to the end of transcription when the promoter remained active. In the no-pause model, r_{ON} is constant from start to finish while the promoter remains active. Therefore, this definition holds true in the Equation 2. However, in the pause-site model, we need to find the location of the first RNAPs at t = 90 s, x_{90}, and use Equation 4.

$$r_{ON} = \frac{3072 - x_{90}}{T_{ON} - 90} \tag{4}$$

We estimated x_{90} from RNAP trajectory (blue) shown in Figure S2F for each T_{ON} measured. This x_{90} is used to calculate r_{OFF}.

$$r_{OFF} = \frac{3072 - x_{90}}{T_{ON \rightarrow OFF} - 90} \tag{5}$$

Here, the means of x_{90} and $T_{ON \rightarrow OFF}$ were used and the error for r_{OFF} was calculated by propagation of standard deviations of x_{90} and $T_{ON \rightarrow OFF}$.

FISH data analysis

Cell outlines were generated from phase contrast images, using the open-source image analysis software MicrobeTracker (Sliusarenko et al., 2011). We used the spotFinder tool in MicrobeTracker to identify fluorescent spots in fluorescence images and quantify their intensities. The same set of parameters (see Data and Code Availability) was used to identify spots from different time points and days of experiments.

To determine the average fluorescence intensity of Z5 and Z3 from a single mRNA, we measured the fluorescence spot intensity of Z5 and Z3 under repressed condition (no IPTG) (Jones et al., 2014; So et al., 2011). The distribution of spot intensities (i.e., integrated intensity of the Gaussian fit to each spot) at t = 0 s in each time-course experiment was approximately bimodal for both Z5 and Z3 cases. The majority of the population fell in the first mode with a mean value about half of that of the second, minor mode, although the actual mean values varied slightly day-to-day. We applied a Gaussian mixture model to extract the means of the two population modes and used the mean of the major mode as the intensity of a single mRNA (either Z5 or Z3). Then, the fluorescence intensities of spots detected at any time point were divided by the single-mRNA signal measured from the same time-course experiment.

To quantify mRNA numbers per cell, we used two methods: one based on the sum of spot intensities within a cell and the other based on the total fluorescence within a cell. In the total-spot-intensity method, normalized spot intensities were summed within cells. In the total-fluorescence method, the total, background-subtracted fluorescence signal within a cell outline (obtained using the inthist function in MicrobeTracker) was divided by the single-mRNA signal. We primarily used the total-spot-intensity method, because it outperformed when cells contained spatially well-separated spots (early time points of induction). However, it underestimated mRNA numbers at later time points when spots overlapped with each other within a cell. Therefore, we used the total-fluorescence method when there were many mRNAs within a cell, such as at steady state from continuous induction (Figures 5A and 5B).

The apparent transcription elongation rate was calculated from each day's Z5 and Z3 data. Specifically, we performed a least-squares fitting of a line to the initial increase in Z5 and Z3 signals and identified the intercepts to the basal levels. The time to transcribe from the Z5 to the Z3 probe regions was then obtained from the time it takes between the appearances of the Z5 and Z3 signals (i.e., the difference between intercepts). The mean and standard deviation of r were calculated from at least three experiments. For Figures 1E, 2D, 4C, 4E, 4F, 5A, 5C, S3C, S5B, and S6A, we consolidated the Z5 and Z3 data from multiple days by randomly sampling an equal number of cells from each day's dataset. The mean and the standard error of the mean (SEM) of the mRNA signals were then calculated from the bootstrapped data.

To analyze the fraction of RNAPs that prematurely terminated during transcription of *lacZ*, we compared the amount of Z3 synthesis relative to that of Z5. In the ON experiments (continuous induction), the Z5 and Z3 mRNA levels reached steady state, as transcription balanced mRNA degradation (e.g., 0.05 mM IPTG in Figure 5A). As the mean lifetimes of Z5 and Z3 regions are similar to each other (Figures S6A–S6C), any difference in plateau levels in Z5 and Z3 mRNAs can be explained by premature termination. In the ON → OFF experiments (promoter repression at t = 90 s), the mRNA level returned to 0 at the end of the time course (after $t \sim 7$ min) due to mRNA degradation (Figure 5C). In this case, we obtained the total amount of *lacZ* mRNA synthesis by compensating for the amount of mRNAs that had been degraded. Specifically, we calculated the total number of Z5 and Z3 mRNA regions synthesized until a certain time point using FISH data and mean mRNA lifetime. We assumed that mRNA present at a given time point (i.e., FISH data) is equal to mRNA produced until that time point minus the mRNA decayed until then. Since the latter could be calculated based on the mean lifetime of the Z5 and Z3 mRNA regions, we back-calculated the total mRNA produced until each time point. Our calculation was based on the following equation of mRNA production and degradation:

$$\frac{dS(t)}{dt} = P(t) - k_{deg}S(t) \tag{6}$$

Here, $S(t)$ is the Z5 or Z3 mRNA present at a given time, measured by single-molecule FISH. $P(t)$ is defined as the rate of mRNA production. k_{deg} indicates the rate of mRNA degradation, measured as the inverse of the mRNA lifetime extracted by fitting an

exponential decay function to the FISH data after promoter repression (Figures S6A–S6C). Since the amount of mRNA produced until time t is the integral of the production rate, or $P(t)$, we have:

$$\int_0^t P(\tau)d\tau = k_{deg}\int_0^t S(\tau)d\tau + S(t) - S(0) \quad (7)$$

We calculated the right-hand side based on $S(t)$ and k_{deg}. For integration, we used the trapz function in MATLAB (Mathworks).

mRNA fold change from qPCR

The fold change in mRNA levels over the transcription reaction time was calculated by the efficiency-corrected ΔCt method (Bookout et al., 2006). Ct stands for cycle threshold, where the fluorescent signal crosses a threshold. ΔCt was calculated by subtracting each sample's Ct with Ct from time-zero sample as a reference, and the primer efficiency was determined from each qPCR curve (Liu and Saint, 2002).

NET-seq data analysis

Larson et al. (2014) reported 3′ nascent mRNA reads for the genome of *E. coli* MG1655 *rpoC::*3XFLAG (RL2081) in the early log phase. In this study, cells were grown at 37°C in MOPS EZ rich defined medium, supplemented with 0.2% glucose (Teknova) and 1 mM IPTG for maximal induction of *lacZ*. We analyzed their data (GEO accession: GSE56720 and GSM1367304) to estimate the RNAP density per gene (code: NETseqAnalysis).

Since the raw data contains 3′ mRNA reads at each nucleotide position from one sample, we calculated the sum of the 3′ mRNA reads within a coding region and divided the result by the length of the coding region ("hits/nt") as a proxy for the relative RNAP density across the genome (Figure S1E). A total of 4,225 genes showing at least one read within their coding region were analyzed and included in the plot. A few gene names were added to the plot as references. As expected, ribosomal genes were among the genes with the highest RNAP densities.

Statistical test

One-sample and two-sample unpaired Student's t tests were performed by using the MATLAB ttest and ttest2 functions, respectively (Table S5).

DATA AND CODE AVAILABILITY

All computer code and parameter sets used in this study can be found at https://github.com/JacobsWagnerLab/.

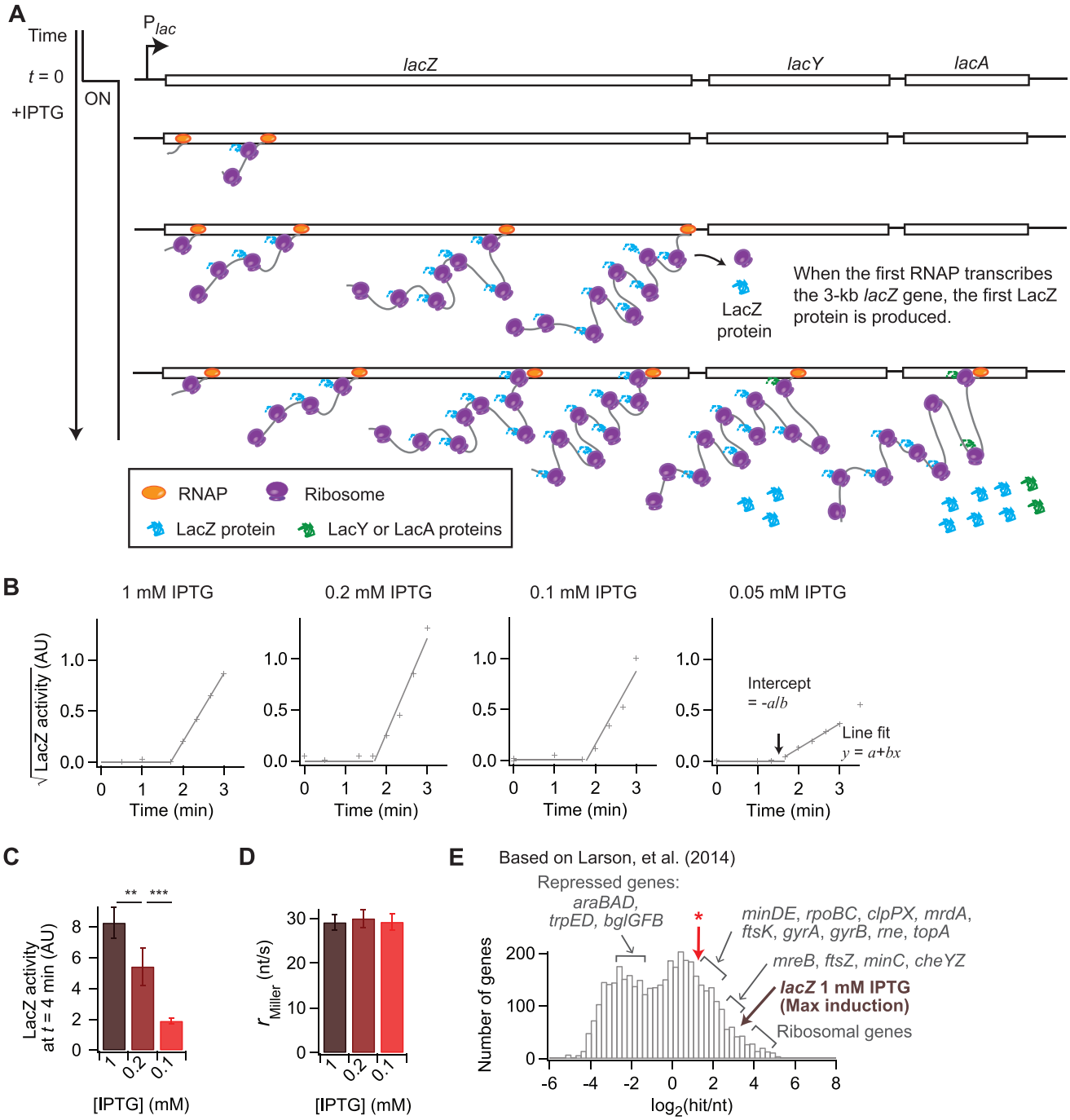

Figure S1. Transcription Elongation Rates and RNAP Densities, Related to Figure 1

(A) Schematic showing transcription and translation kinetics of the *lac* operon following IPTG addition. At time zero (top), IPTG is added to turn on the *lac* promoter. Next, RNAPs start to transcribe the *lac* operon. As soon as the ribosome-binding site is transcribed, ribosomes load onto the nascent mRNA and start translation. When the first RNAP reaches the end of the *lacZ* gene, the associated ribosome produces the first LacZ protein. Thereafter, LacZ proteins rapidly accumulate. We calculated the apparent elongation rate of transcription and translation in *E. coli* using the time point at which LacZ proteins first appear and start accumulating, as previously done (Jin et al., 1992; Kepes, 1969; Proshkin et al., 2010; Schleif et al., 1973).

(B) Example traces of the square root of LacZ activity following IPTG addition. Shown are examples of data points (+) and two-line least-squares fits (solid lines) obtained under different IPTG concentrations using the Miller assay. AU indicates arbitrary units.

(C) LacZ activity level measured with the Miller assay. Varying concentrations of IPTG were used to induce the expression of *lacZ* in MG1655 cells grown at 37°C in supplemented MOPS EZ rich defined medium. Higher IPTG concentrations were needed to obtain a fourfold change in promoter activity compared to our default

(legend continued on next page)

growth condition (M9glyCaaT at 30°C; Figure 1A), possibly because of the temperature difference, but most probably because the MOPS EZ rich defined medium contains glucose (0.2%), an anti-inducer of the *lac* promoter. Error bars are standard deviations of at least three experiments. ** and *** indicate $p \leq 0.01$ and $p \leq 0.001$, respectively (two-sample t test; Table S5).

(D) Measurements of apparent transcription elongation rates under conditions described in (C). Error bars are standard deviations of at least three experiments.

(E) Relative RNAP density per gene based on published genome-wide RNAP profiling in *E. coli* (Larson et al., 2014) performed under the same growth conditions as in (C) and (D). See STAR Methods for the method of analysis. The fully induced (1 mM IPTG) *lacZ* gene (brown arrow) has lower RNAP density than ribosomal genes, but higher RNAP density than genes that are critical for cell physiology, such as those involved in cell morphogenesis and division (*mreB*, *ftsZ*, and *minCDE*), chemotaxis (*cheYZ*), transcription (*rpoBC*, *topA*, *gyrA* and *gyrB*), mRNA degradation (*rne*), protein degradation (*clpXP*) and peptidoglycan cross-linking (*mrdA*). The red arrow with an asterisk indicates a fourfold lower RNAP density than that of maximally induced *lacZ* (1 mM IPTG). Assuming that RNAP density scales with promoter activity, a fourfold lower RNAP density corresponds to *lacZ* induction for which the apparent speed of RNAP is the same as for maximally induced *lacZ* (D). Genes known to be repressed or weakly expressed under the experimental condition, such as *araBAD* and the *trp* and *bgl* operons, displayed very low RNAP density, as expected.

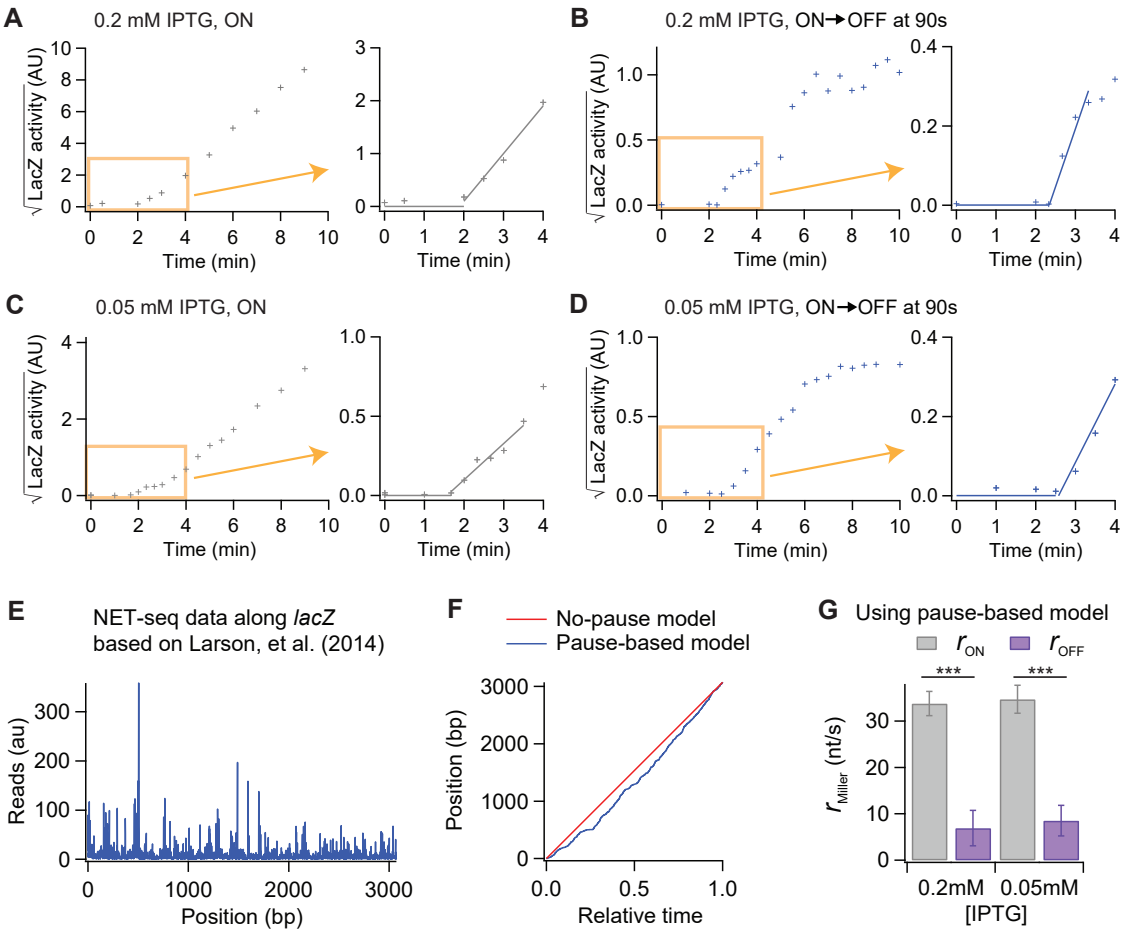

Figure S2. Apparent RNAP Slowdown after Promoter Repression, Related to Figure 2

(A-D) Representative plots of LacZ activity over time depending on promoter activity. Shown are example traces of the square root of LacZ activity over time in a single experiment (+ shows the raw data) and the two-line fits (solid lines) in the zoomed regions (yellow rectangles). AU indicates arbitrary units. Experimental conditions were as follows: MG1655 cells were grown in M9glyCaaT at 30°C. After induction with 0.2 mM (A, B) or 0.05 mM (C, D) IPTG, the promoter was either kept active (A, C) or turned off 90 s after IPTG addition (B, D). For promoter repression, we used 5 mM ONPF in the case of 0.05 mM IPTG. This concentration of ONPF was insufficient to turn off the *lac* promoter induced with 0.2 mM IPTG, which we circumvented by using 500 mM glucose. Note that when the promoter was turned off (B, D), the LacZ production leveled off after $t \sim 6$ min.

(E) RNAP enrichment in the fully-induced *lacZ* coding region, based on published data (Larson et al., 2014). Reads at each nucleotide position reflect relative dwell time of RNAPs at the position.

(F) Calculated trajectories of an RNAP transcribing *lacZ*, assuming no pause (red) or site-specific pausing (blue) based on the data shown in (E). See STAR Methods for a description of the no-pause-site and pause-site models used for generating these trajectories.

(G) Calculations of r_{ON} and r_{OFF} from the data shown in Figure 2A using the pause-site model. Error bars were calculated based on standard deviations of replicates described in Figure 2A and propagation of error in r_{OFF} calculation (see STAR Methods). *** indicates $p \leq 0.001$ (two-sample t test).

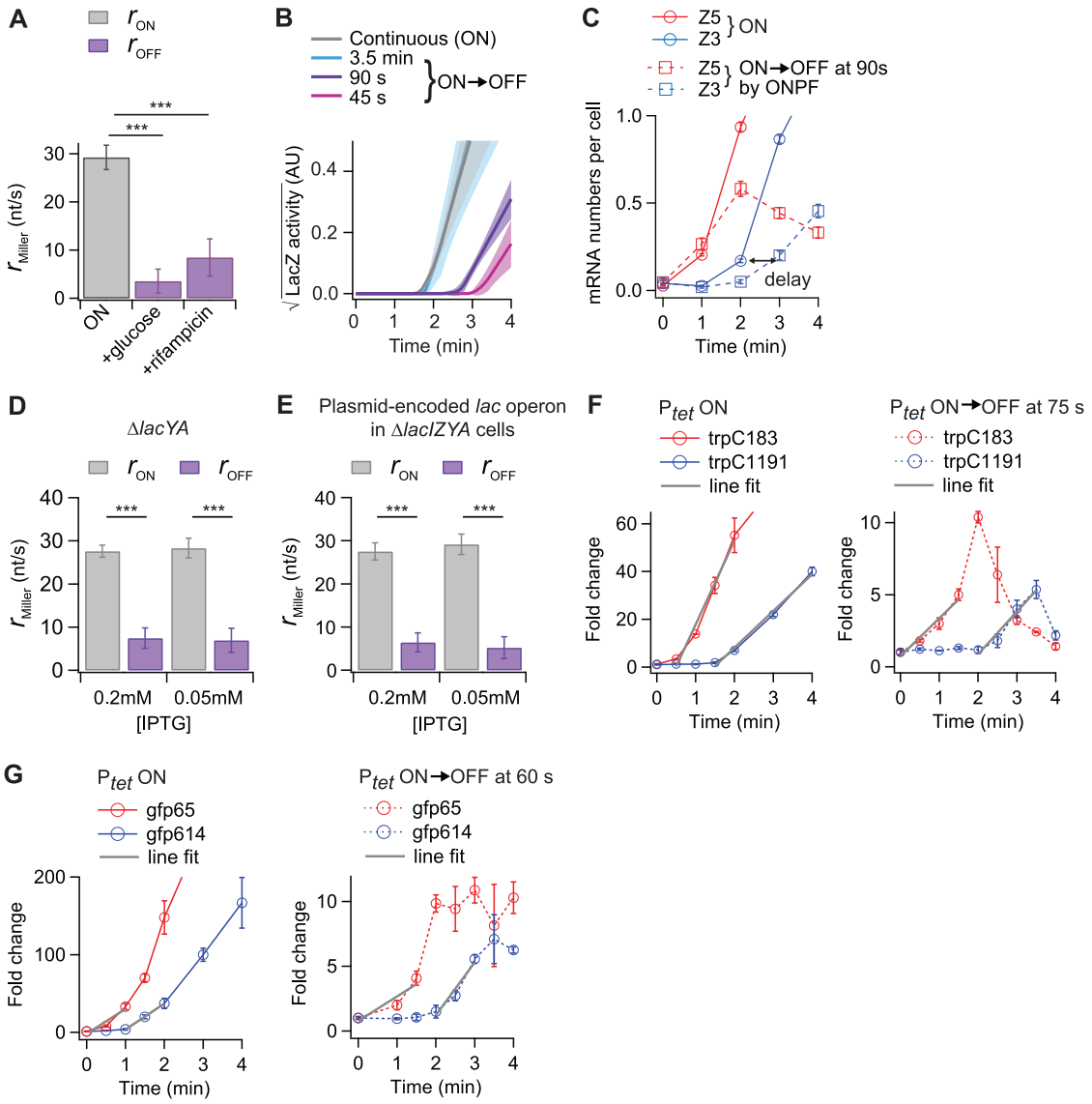

Figure S3. Robustness of the Apparent RNAP Slowdown after Promoter Repression across Various Conditions, Related to Figure 2

(A) Apparent transcription elongation rate of *lacZ* following promoter repression by different means. The expression of *lacZ* in *E. coli* cells (MG1655 grown in M9glyCaaT at 30°C) was induced with 0.05 mM IPTG at $t = 0$ s and the promoter either remained active (ON) or was turned off (OFF) by adding 500 mM glucose at $t = 90$ s or 400 μg/mL rifampicin at $t = 40$ s. Rifampicin was added earlier because its penetration into the cells appears delayed (Montero Llopis et al., 2010). Error bars are based on standard deviations of at least four experiments for each condition and propagation of error in r_{OFF} calculation. *** indicates a statistically significant difference ($p \leq 0.001$, two-sample t test). See Table S5 for *P values*.

(B) Kinetics of the square root of LacZ activity following IPTG addition and promoter repression. Cell growth and *lacZ* induction were the same as in (A). ONPF (5 mM) was added at indicated times for promoter repression. Lines and shaded areas indicate means and standard deviations of two-line fits done on each time-course experiment. Promoter repression at $t = 3.5$ min did not show significant delay in the synthesis of the first LacZ proteins as expected, since the promoter was turned off after the initial LacZ protein appearance. Turning off the promoter earlier at $t = 45$ s, compared to $t = 90$ s, showed further delay in the appearance of the first LacZ proteins. A total of 13, 10, 11 and 6 experiments were performed for continuous promoter activity (ON), or repressed promoter activity (ON → OFF) at 3.5 min, 90 s, and 45 s, respectively.

(C) Z5 and Z3 mRNA numbers per cell over time in FISH microscopy experiments, in which the promoter remained active or was turned off by addition of 5 mM ONPF at $t = 90$ s. Cell growth and *lacZ* induction were the same as in (A). The black arrow qualitatively indicates the delay in Z3 appearance from the basal level in the promoter-repression (ON → OFF) case relative to when the promoter remains active (ON). At least 6000 (ON) and 2000 (ON → OFF) cells were analyzed per time point. Error bars are bootstrapped standard errors of the mean.

(D) Apparent transcription elongation rate of *lacZ* measured in the Δ*lacYA* strain CJW5461 (M9glyCaaT, 30°C) using the Miller assay under the condition of continuous induction (ON) or promoter repression at $t = 90$ s (ON → OFF), either with 500 mM glucose (for 0.2 mM IPTG) or 5 mM ONPF (for 0.05 mM IPTG). Error bars are based on standard deviations of at least three experiments for each condition and propagation of error in r_{OFF} calculation. *** indicates a statistically significant difference ($p \leq 0.001$, two-sample t test). See Table S5 for *P values*.

(legend continued on next page)

(E) Apparent transcription elongation rate of *lacZ* measured in CJW5616 cells (M9glyCaaT, 30°C), in which the *lac* operon is encoded on the low-copy plasmid pEXT22 (Dykxhoorn et al., 1996). The Miller assay was used under the condition of continuous induction (ON) or promoter repression at t = 90 s (ON → OFF), either with 500 mM glucose (for 0.2 mM IPTG) or 5 mM ONPF (for 0.05 mM IPTG). Error bars are based on standard deviations of at least three experiments for each condition and propagation of error in r_{OFF}. *** indicates a statistically significant difference ($p \leq 0.001$, two-sample t test). See Table S5 for *P value*s.
(F) *trpC* mRNA production in CJW6986 cells grown in LB at 25°C. Expression of *trpC* (under P_{tet}) was induced by 100 ng/mL aTc at t = 0 s. The promoter remained active (ON) or becomes repressed (ON → OFF) by addition of 400 μg/mL rifampicin at t = 75 s. The fold change in specific mRNA regions was measured by qPCR (see STAR Methods). Primers trpC181 and trpC1191 bind 181-nt and 1191-nt away from the start of the open reading frame, respectively (see Table S4 for primer sequences). Error bars are standard deviations of replicates. Raw data are shown with line fits (gray lines).
(G) *gfp* mRNA production in CJW6919 cells grown in M9glyCaaT at 25°C. Expression of *gfp* (under P_{tet}) was induced by 100 ng/mL aTc at t = 0 s. The promoter remained active (ON) or becomes repressed (ON → OFF) by addition of 400 μg/mL rifampicin at t = 60 s. The fold change in specific mRNA regions was measured by qPCR. gfp65 and gfp614 are primers that bind 65 nt and 614 nt away from the start of the open reading frame, respectively (see Table S4 for primer sequences). Error bars are standards deviation of replicates. Raw data are shown with line fits (gray lines).

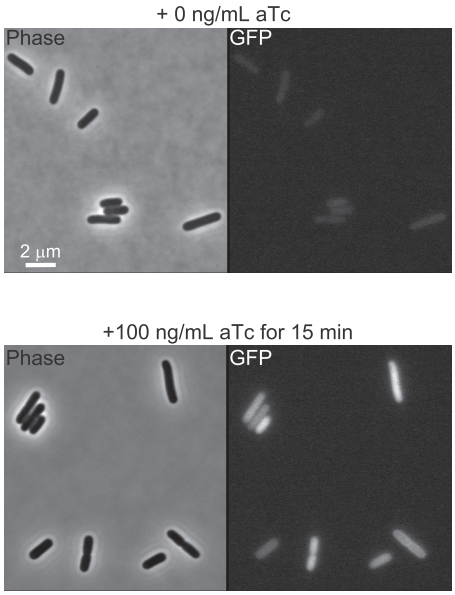

Figure S4. Induction of GFP Synthesis with aTc, Related to Figure 3

Phase contrast and fluorescence images of CJW6919 cells (M9glyCaaT at 30°C) before and 15 min after adding 100 ng/mL aTc (same induction conditions as for the *topA*-overexpression experiments in Figure 3C). The GFP signals were scaled identically for comparison purpose. After 15-min exposure of 100 ng/mL aTc, most cells show fluorescence signal higher than unexposed cells.

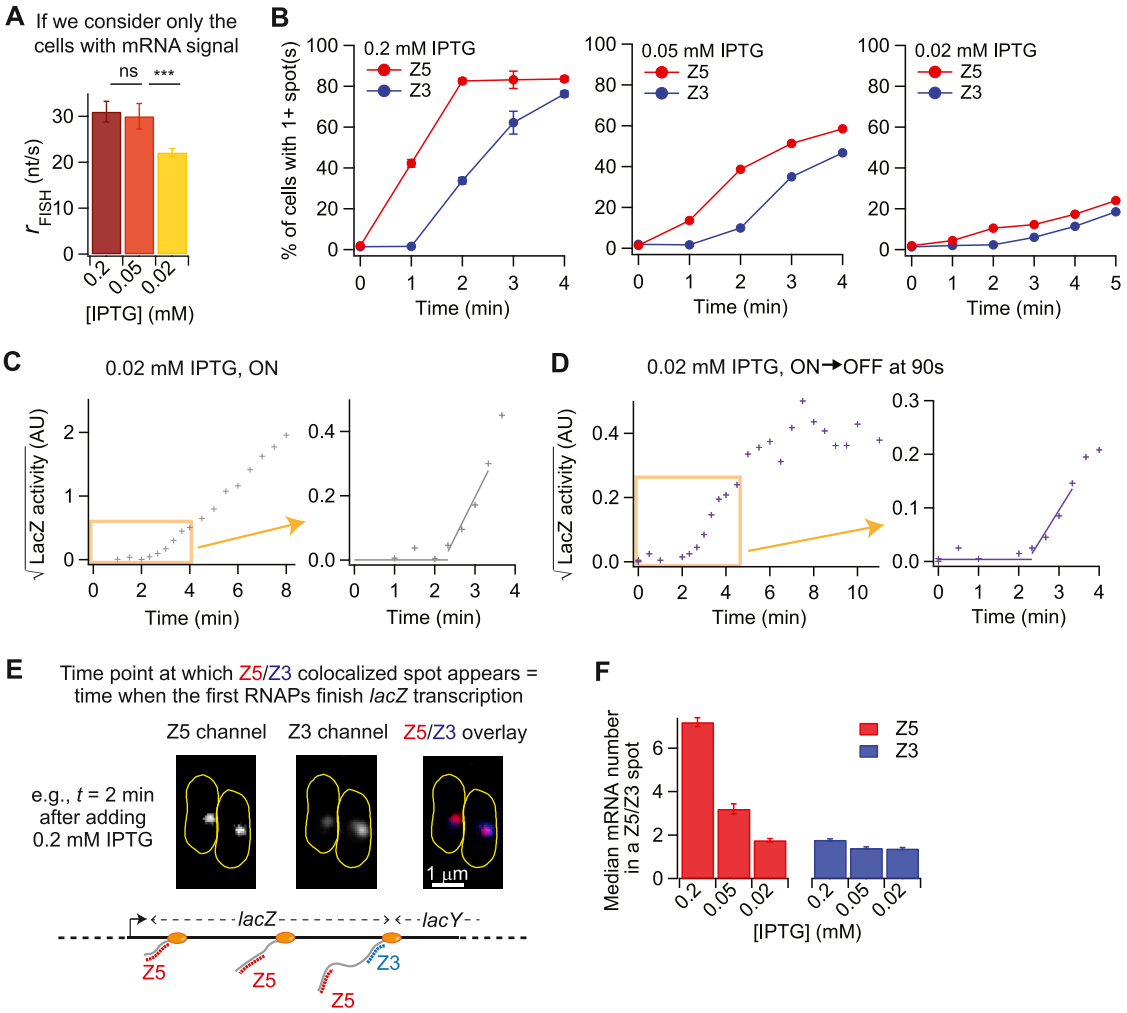

Figure S5. Transcription Elongation Kinetics and Features at Different IPTG Concentrations, Related to Figure 4

(A) Apparent rate of transcription elongation at different IPTG concentrations as determined by analysis of FISH experiments. Unlike the data plotted in Figure 4D, only cells with *lacZ* mRNA signal were considered (n > 120 for each IPTG concentration). Error bars are standard deviations from more than four experiments. *** indicates p ≤ 0.001 (two-sample t test; Table S5) and ns indicates a statistically non-significant difference.

(B) Percentage of cells with one or more *lacZ* mRNA spots after induction with the indicated concentrations of IPTG. Error bars are bootstrapped standard errors of the mean. These statistics were obtained from the same number of cells used in Figures 1E and 4C.

(C) Example traces of the square root of LacZ activity following addition of 0.02 mM IPTG at t = 0 s. AU indicates arbitrary units. The zoomed regions (yellow rectangles) show the two-line fits (solid lines).

(D) Same as (C) except that the promoter was turned off at t = 90 s by 5 mM ONPF. Note that when the promoter was turned off, the LacZ production leveled off after t ~6 min.

(E) Schematic and images illustrating the first time point at which Z5 and Z3 mRNA spots colocalized. When the first RNAPs finished transcription (close to t = 2 min under 0.2-0.05 mM IPTG and close to t = 3 min under 0.02 mM IPTG), Z3 mRNA signal appeared as a spot that colocalized with Z5 mRNA signal. Hence, Z5 mRNA levels in these Z5- and Z3-colocalized spots are related to the number of RNAPs on the DNA when the rate of transcription elongation was measured.

(F) Median Z5 or Z3 mRNA number in Z5- and Z3-colocalized spots when the first RNAPs finish *lacZ* transcription. A total of 841, 285, 442 colocalized spots were obtained and analyzed from experiments with 0.2 mM IPTG (t = 2 min), 0.05 mM IPTG (t = 2 min), and 0.02 mM IPTG (t = 3 min), respectively. Z5 mRNA numbers in colocalized spots decrease with decreasing IPTG concentrations, as expected for a reduction in RNAP density. Z3 mRNA numbers in colocalized spots remain independent of the IPTG concentrations, arguing against the notion of RNAP convoy formation. Error bars are bootstrapped standard errors of the median.

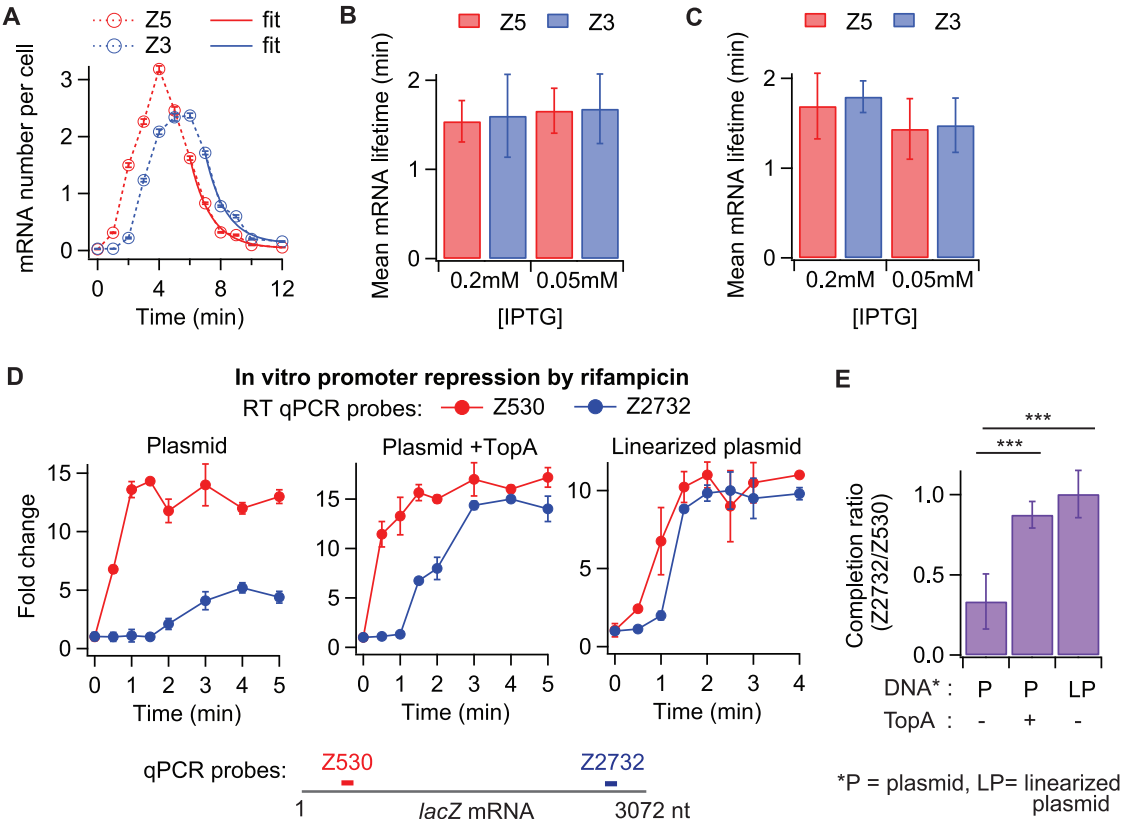

Figure S6. Comparison of Numbers and Lifetimes between the 5′ and 3′ End Regions of the *lacZ* mRNA, Related to Figure 5

(A) Levels of 5′- and 3′ end mRNA regions of the *lacZ* (dotted lines) after promoter repression at $t = 3.5$ min. After *lacZ* expression was induced with 0.05 mM IPTG at $t = 0$ min, 500 mM glucose was added at $t = 3.5$ min. This time point was chosen to ensure that promoter repression happens only *after* the first RNAPs have finished transcription. The decay of the Z5 and Z3 mRNA signals was fit with a single-exponential function (solid lines) to obtain the lifetime of each mRNA region. At least 2500 cells were analyzed per time point. Error bars are bootstrapped standard errors of the mean.

(B) Mean lifetimes of the Z5 and Z3 mRNA regions, as determined by the procedure described in (A). The promoter was turned off at $t = 3.5$ min after induction with IPTG at the indicated concentrations. Error bars are standard deviations of five experiments.

(C) Mean lifetimes of the Z5 and Z3 mRNA regions, measured the same way as in (B), when the promoter was turned off at $t = 90$ s (i.e., *before* the first RNAPs finish transcription of *lacZ*). Error bars are standard deviations of five and eight experiments for 0.2 and 0.05 mM IPTG, respectively.

(D) Transcription of *lacZ* mRNA *in vitro* as described for Figures 2G and 3B. Primers Z530 and Z2732 bind 530 nt and 2732 nt away from the first base of the open reading frame, respectively (see Table S4 for primer sequences). Error bars are standard deviations of replicates. Because the promoter is turned off by rifampicin and there is no RNases degrading mRNAs *in vitro*, Z530 and Z2732 are expected to reach similar plateau levels. However, this expectation was observed only from the linearized plasmid template and the non-linearized plasmid DNA in the presence of TopA.

(E) Completion ratio between the Z530 and Z2732 mRNA regions depending on the *in vitro* transcription reaction conditions described in (D). Error bars are standard deviations of at least three experiments. *** indicates $p \leq 0.001$ (two-sample t test; Table S5).

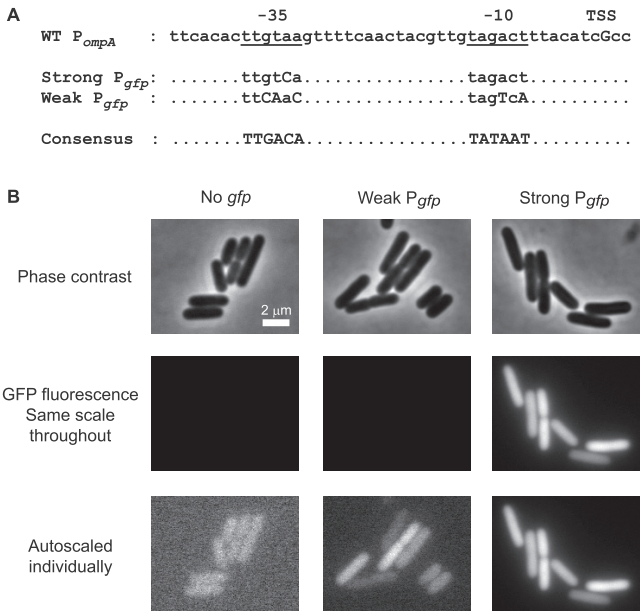

Figure S7. Variable Expression of GFP Using Different Promoter Sequences, Related to Figure 6

(A) DNA sequences for the wild-type *E. coli ompA* promoter (P_{ompA}), the strong *gfp* promoter (strong P_{gfp}), the weak *gfp* promoter (weak P_{gfp}), and the consensus *E. coli* promoter. Strong P_{gfp} was made by introducing a single-base mutation in the −35 region of P_{ompA} to make it more similar to the promoter consensus. Weak P_{gfp} was made by mutating five bases of P_{ompA} to reduce similarity to the promoter consensus.

(B) Phase contrast and corresponding fluorescence images of cells carrying a plasmid lacking an insert (no *gfp*, strain CJW6647) or the same plasmid expressing *gfp* from the strong (CJW6987) or weak (CJW6998) promoter described in (A). Cells were grown in M9glyCaaT at 30°C.